Ocean Engineering 269 (2023) 113578

Contents lists available at ScienceDirect

Ocean Engineering

journal homepage: www.elsevier.com/locate/oceaneng

Fuzzy logic control of an artificial neural network-based floating offshore wind turbine model integrated with four oscillating water columns

Irfan Ahmad *, Fares M'zoughi, Payam Aboutalebi, Izaskun Garrido, Aitor J. Garrido

Automatic Control Group—ACG, Institute of Research and Development of Processes—IIDP, Department of Automatic Control and Systems Engineering, Faculty of Engineering of Bilbao—EIB/BIE, University of the Basque Country—UPV/EHU, Po Rafael Moreno No3, 48013, Bilbao, Spain

ARTICLE INFO

Keywords:
Artificial neural network (ANN)
Floating offshore wind turbines (FOWTs)
Oscillating water column (OWC)
Intelligent control
Fuzzy logic control (FLC)
Vibration mitigation
Active structural control

ABSTRACT

Renewable energy induced by wind and wave sources is playing an indispensable role in electricity production. The innovative hybrid renewable offshore platform concept, which combines Floating Offshore Wind Turbines (FOWTs) with Oscillating Water Columns (OWCs), has proven to be a promising solution to harvest clean energy. The hybrid platform can increase the total energy absorption, reduce the unwanted dynamic response of the platform, mitigate the load in critical situations, and improve the system's cost efficiency. However, the nonlinear dynamical behavior of the hybrid offshore wind system presents an opportunity for stabilization via challenging control applications. Wind and wave loads lead to stress on the FOWT tower structure, increasing the risk of damage and failure, and raising maintenance costs while lowering its performance and lifespan. Moreover, the dynamics of the tower and the platform are extremely sensitive to wind speed and wave elevation, which causes substantial destabilization in extreme conditions, particularly to the tower top displacement and the platform pitch angle. Therefore, this article focuses on two main novel targets: (i) regressive modeling of the hybrid aero-hydro-servo-elastic-mooring coupled numerical system and (ii) an ad-hoc fuzzy-based control implementation for the stabilization of the platform. In order to analyze the performance of the hybrid FOWT-OWCs, this article first employs computational Machine Learning (ML) techniques, i.e., Artificial Neural Networks (ANNs), to match the behavior of the detailed FOWT-OWCs numerical model. Then, a Fuzzy Logic Control (FLC) is developed and applied to establish a structural controller mitigating the undesired structural vibrations. Both modeling and control schemes are successfully implemented, showing a superior performance compared to the FOWT system without OWCs. Experimental results demonstrate that the proposed ANN-based modeling is a promising alternative to other intricate nonlinear NREL 5 MW FOWT dynamical models. Meanwhile, the proposed FLC improves the platform's dynamic behavior, increasing its stability under a wide range of wind and wave conditions.

1. Introduction

Transmission and distribution infrastructures use a considerable amount of renewable energy to complement traditional global energy (Akinbami et al., 2021; Souissi, 2021). It has several advantages over conventional energy sources. For example, the induction of various renewable energy sources (wind, solar power, biomass gasifiers) and storage devices shows a reduction in the Levelized Cost of Electricity (LCOE) from 20% to 40% (Tomin et al., 2022). It improves the quality of electricity supply to the analyzed settlements. Therefore, researchers are trying to make renewable energy generation cheaper to compete with conventional energy generation and attract investors (Khan et al., 2022). Renewable energy installations broke new records in 2021, as illustrated in Fig. 1, according to the International Energy Agency (IEA). It is estimated that they will continue to increase by 8%, reaching almost 320 GW every consecutive year (IEA, 2017).

Marine energy production aims to reach an annual growth of over 25% (Kulkarni and Edwards, 2022). Infrastructures for generating wind-powered and wave-powered electricity are increasingly popular, and both technologies are expected to contribute more to the European energy market (Ravinuthala et al., 2022). FOWTs are the primary component of this energy sector due to low visual disturbances,

* Corresponding author.
E-mail addresses: irfanahmad.irfan@ehu.eus (I. Ahmad), fares.mzoughi@ehu.eus (F. M'zoughi), payam.aboutalebi@ehu.eus (P. Aboutalebi), izaskun.garrido@ehu.eus (I. Garrido), aitor.garrido@ehu.eus (A.J. Garrido).

https://doi.org/10.1016/j.oceaneng.2022.113578
Received 4 October 2022; Received in revised form 1 December 2022; Accepted 27 December 2022
Available online 3 January 2023

availability, high potential, and superior wind quality. Several ocean energy innovations, especially tidal and wave conversion systems, have emerged to generate a substantial amount of clean energy (Dawoud, 2021).

The fundamental difficulty in developing offshore floating renewable energy structures is to withstand the harsh wind and ocean environment while remaining commercially viable in a chaotic and competitive global market (Papi and Bianchini, 2022). The structural behavior of FOWTs in deep water environments may vary rapidly over time due to the extremely dynamic operating conditions. However, the high cost of operation and maintenance (O&M) for these complex structures is a significant issue that motivates scholars to investigate emerging trends from technical and financial perspectives to improve these structures' reliability, maintenance, and optimization (Bortolotti et al., 2022). Furthermore, the stress and fatigue induced by the wind turbine produce unwanted vibrations, which lead to efficiency loss, structure imbalance, and, eventually, equipment breakdowns (McMorland et al., 2022).

There are several approaches for reducing platform vibrations. However, passive or active structural control is the most convenient method for reducing the load on FOWTs (Lackner and Rotea, 2011a; Sierra-García and Santos, 2020). A recent analysis of FOWTs control systems, outlining the benefits and shortcomings of the most popular control algorithms, has been demonstrated in (López-Queija et al., 2022). Some methods for barge platform stabilization are Tuned Mass Dampers (TMD) (Coudurier et al., 2015), inerters (Zhang and Høeg, 2021), Liquid Mass Dampers (LMD) (Dinh and Basu, 2015), and mooring lines adjustment (Borg et al., 2014).

2. Wind-wave hybrid platform review

In the last decade, several research groups started their endeavors to combine wave energy converters with FOWTs to harness energy. Integrating FOWTs with OWCs wave energy converters has been revealed as a promising solution for hybrid renewable energy production because OWCs combined into the FOWTs structure not only enable platform stabilization but also increase the quantity and quality of the energy to be harvested. The OWC works on the principle of a closed chamber with an opening below that allows water to flow up and down in response to incoming waves. The air inside the chamber is compressed and decompressed, propelling self-rectifying air turbines located at the top of the chambers. Various types of WECs can be found in Europe, including the NEREIDA Wave Power Plant in Mutriku in Spain (Torre-Enciso et al., 2009) and Limpet in Scotland (Heath et al., 2001).

D. Zhang et al. developed coupled numerical framework modeling in the time domain for a FOWT integrated with OWCs into a semi-submersible floating platform (Zhang et al., 2022). The article (Sarmiento et al., 2019) describes the experimental work carried out to validate a new floating semisubmersible structure that combines three oscillating water columns with a 5 MW wind turbine and wind harvesting (5-MW wind turbine). Recently, a hybrid platform used to generate energy from both wind and waves has been validated by researchers (M'zoughi et al., 2021). They demonstrated the feasibility of integrating two and four OWCs in barge platforms (Aboutalebi et al., 2021). As illustrated in Fig. 2, integrating four OWCs into a platform proves to be a potential strategy that can be used for active structural control. Compared to spar and tension leg platforms (Lin et al., 2019), the platform's size and design make it easier to provide space for Wave Energy Converter (WEC) integration.

Neural networks are frequently used in pattern recognition and classification because they are nonlinear dynamical systems capable of nonlinear mapping functions. Numerous researchers employ adaptive strategies for the stability of wind turbine platforms, such as genetic algorithms, artificial intelligence, and meta-heuristic algorithms (Sacie et al., 2022). Hybrid offshore systems use a range of sensors to measure vibration, temperature, humidity, and other characteristics. These tools monitor every parameter to ascertain the state of each component of the system. After that, the model development process is initiated by employing robust algorithms. A significant amount of data may be processed using machine learning algorithms, with ANNs being one of the most popular techniques for modeling such nonlinear (JiménezAlfredo et al., 2017) systems. Numerous regression-oriented approaches have been applied with different training functions (Guo et al., 2016). The Levenberg-Marquardt (Sitharthan et al., 2017) and Bayesian regularization (Jazayeri et al., 2016) backpropagation algorithms are regarded as the best candidates for such nonlinear dynamics since fast backpropagation techniques are strongly recommended as first-choice supervised algorithms. This leads to various researchers' employment of ANN-oriented methods to improve the overall performance of floating structures. Some advantages of using ANN are adaptive learning, self-organization, fault tolerance, online operation, and system integration flexibility. For example, researchers (Salcedo-Sanz et al., 2009) have developed a multilayer perceptron (MLP)-based method to predict wind speed at various locations within a wind farm. They showed that this method produces mean absolute error levels with the lowest possible values in a real wind farm. Different models, including two-layer ANN (Cadenas and Rivera, 2009), IRBFNN (Chang et al., 2017), RBFNN (Noorollahi et al., 2016), nonlinear adaptive model (Kaur et al., 2016), a set of mixed-density ANN networks (Men et al., 2016), neural networks along with reinforcement learning in the control of wind turbines (Sierra-García and Santos, 2021), are used by various researchers in forecasting short-term wind speeds.

Unpredictable wave-wind flow may reduce power generation efficiency. Several researchers have introduced several algorithms to provide rotational speed control for FOWTs. For example, J. Jonkman et al.

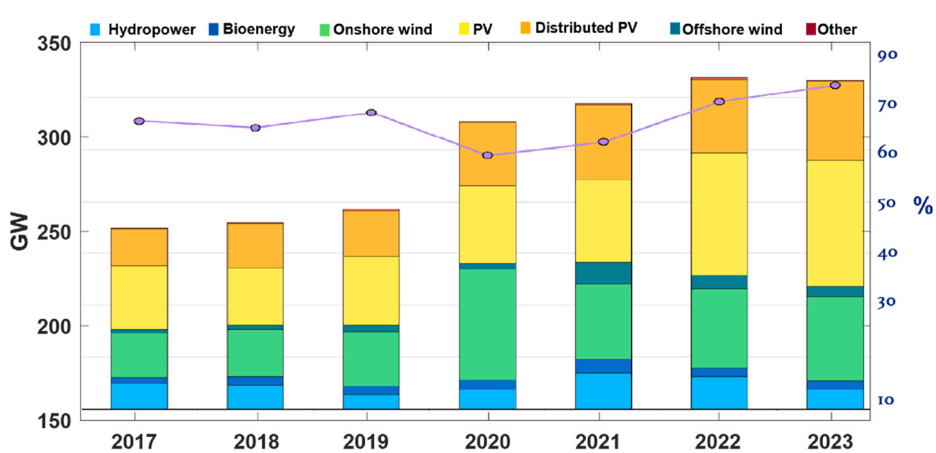

Fig. 1. Net renewable capacity additions by technology (2017–2023), (IEA, 2017).

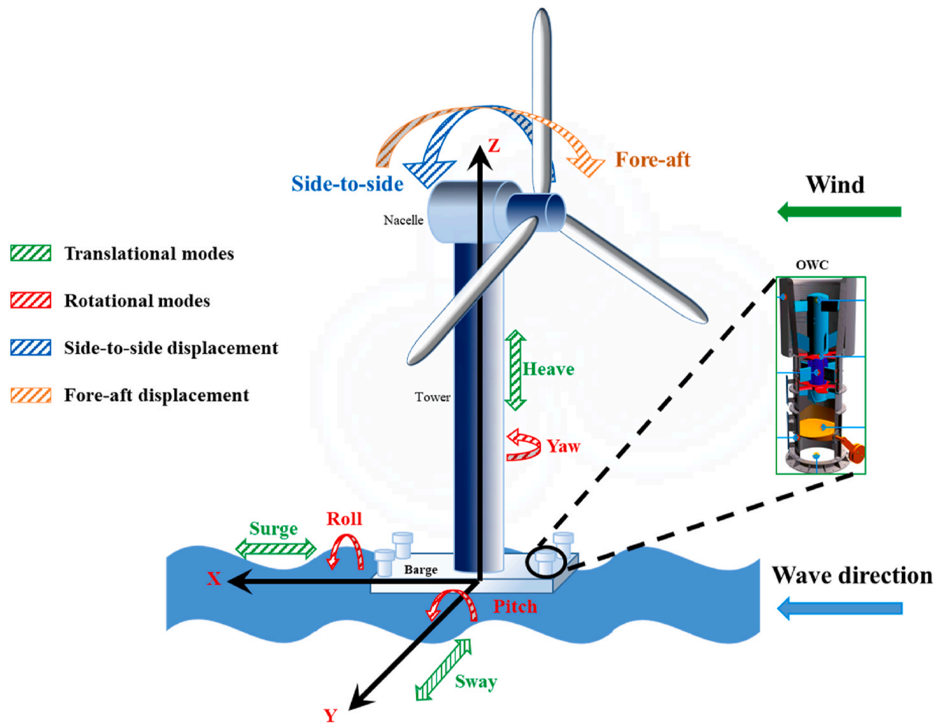

Fig. 2. Proposed Hybrid FOWT-OWCs system.

(Jonkman and Buhl, 2005) used a gain-scheduled proportional-integral technique to develop the OpenFAST (Fatigue, Aerodynamics, Structures, and Turbulence) simulator. They designed a baseline collective blade pitch controller for three primary floating wind turbines (Zhang et al., 2019). An active control strategy called a Translational Oscillator with a Rotational Actuator (TORA) has been proposed to mitigate vibrations (Shah et al., 2021a). M.A. Lackner et al. (Stewart and Lackner, 2013) developed FAST-SC, which allows structural control of FOWTs. However, most active, passive, blade, torque, and rotational speed control strategies have been developed using OpenFAST (Lackner and Rotea, 2011b) (e.g., TMD). Platform stability has been improved by implementing a Proportional Integral Derivative (PID) supplemental airflow control approach to control valves inside OWCs (Maria-Arenas et al., 2019). An adaptive neuro-fuzzy inference system (ANFIS), a hybrid system for power optimization control, is utilized to track the maximum power points and calculate the power coefficients (Mishra et al., 2020). To reduce the error between the required value and the measured value, PID is used in collective torque control (M'zoughi et al., 2020; Amundarain et al., 2011). The negative dampening effect is a challenge that emerges and requires the best possible control of the blades. Besides, using an FLC for the same application is significantly less expensive, easier to recognize and adjust, and customizable using natural linguistic expressions. Therefore, FLCs are preferred over traditional controllers because they are more robust and can withstand a broader range of operating conditions than other model-based controllers (Shah et al., 2021b). FLC is an excellent control strategy that presents a just-in-time reaction, fast to noises, disturbances, and transients (Zadeh, 1996; M'zoughi et al., 2018).

All the above-mentioned modeling strategies are for FOWTs with semisubmersible structures in the time or frequency domain. Moreover, understanding the aero-hydro-servo-elastic performance of floating offshore structures is an intricate and challenging task. When a new wave energy converter is incorporated into the FOWT's platform, it modifies the dynamical complexity. Therefore, efficient, intelligent machine learning modeling and control are necessary to evaluate the performance of innovative designs and to mimic the behavior of the complex hybrid dynamics of FOWT-OWCs, thus allowing the implementation of feedback controls. Therefore, this article has dual objectives; firstly, developing a novel control-oriented regressive model for hybrid design. Secondly, using estimated models to implement a Fuzzy feedback control with numerical tools using air valves to ensure stability for the entire system.

The remainder of the paper is as follows: Section III describes all the subsystems of the FOWT-OWCs system and mathematical models. The proposed hybrid platform geometry design models and related hydrodynamic calculations are covered in Section IV. Section V describes the suggested FLC for platform pitch and tower fore-aft control to alleviate unwanted vibrations. The experimental results and their cross-pounding validation are presented in Section VI. Finally, the last section ends with conclusions and future recommendations.

3. Theoretical background

3.1. Wave elevation model

A simplified model of wave elevation is a unidirectional regular sine wave whose surface dynamics are explained by the Airy wave theory (Falcão and Justino, 1999).

$$z_{\omega}(t) = A\sin(\omega t) = A\sin(2\pi f t) = A\sin\left(\frac{2\pi}{\lambda}ct\right) \tag{1}$$

where $c = f\lambda$ is defined as propagation velocity,A is the wave amplitude from Still Water Level (SWL) and λ is calculated by measuring the distance between two consecutive waves. From Eq. (1), a wave's temporal variation is a macroscopic representation of the oscillating motion of water molecules at a particular location. A new variable representing the spatial dimension in the wave's front direction is provided to enable the oscillating behavior to be applied to any place on the wave's surface. Eq. (1) can be modified as follows:

$$z_{\omega}(x,t) = A\sin\left(\frac{2\pi}{\lambda}(ct - x\theta)\right) = \frac{H}{2}\sin(\omega t - kx\theta) \tag{2}$$

where wave number $K = \frac{2\pi}{\lambda}$ and H is wave height, x is directed with the direction of wave propagation and θ represents the wave angle in the direction of x-axis. As explained below, it can be generalized by superposing an n-fold number of waves (De O Falcão and Rodrigues, 2002).

$$z_{\omega}(x,t) = \sum_{i=1}^{N} K_i \sin(\omega_i t - k_i + \theta_i) \tag{3}$$

$$K_i = \sqrt{2S_i \Delta\omega_i} \tag{4}$$

where N is the number of waves, S_i is the spectral density, k_i is the number of each wave component and ω_i is the angular frequency. The two most widely recognized theoretical wave spectra are the Bretschneider spectrum for fully developed waves and the JONSWAP spectrum for partially developed waves. The generalized representation of the spectrum can be expressed as (Sheng et al., 2017),

$$S_i(\omega_i) = (1 - 0.287\ \ln(\gamma))\frac{5\omega_p^4}{16\omega^5}K_s^2\gamma^{\beta}e^{\frac{5\omega_p^4}{16\omega^5}} \tag{5}$$

where β is $\exp\left(-\frac{(\omega-\omega_p)^2}{2\omega_p^2\alpha^2}\right)$ and $\alpha = \left\{\begin{matrix} 0.07, if\ \omega \le \omega_p \\ 0.09, if\ \omega \le \omega_p \end{matrix}\right\}$, K_s is the wave height, ω_p is the peak angular frequency. Depending on the wave condition, a value between 1 and 5 is chosen for the heat ratio parameterγ. The value of the standard JONSWAP spectrum γ is 3.3 (Goda, 1999).

3.2. Wind turbine

The turbine is a system of machinery that converts wind energy into mechanical energy; a generator converts mechanical energy to electrical energy. Output power and torque may be defined as (Jonkman et al., 2009):

$$P_w = \frac{1}{2}C_P(\vartheta,\lambda)\rho\pi r^2 v_{wind}^3 \tag{6}$$

$$Q_w = \frac{1}{2}C_Q(\vartheta,\lambda)\rho\pi r^2 v_{wind}^3 \tag{7}$$

where C_p, and C_Q are the power and torque coefficient, ρ and r are the air density (kg/m^3) and wind rotor radius (m). ϑ is the blade pitch angle in (degree). The tip-speed ratio (TSR) λ can be defined as:

$$\lambda = \Omega_t \frac{R}{V_{wind}} \tag{8}$$

where Ω_t is the rotational speed of the turbine in ($rad/\ s$). The power coefficient is the nonlinear function of ϑ and λ that can be defined as:

$$\begin{cases} C_p(\vartheta,\lambda) = 0.22\left(\frac{116}{\lambda_i} - 0.4\vartheta - 5\right)e^{-12.5/\lambda_i} \\ \frac{1}{\lambda_i} = \frac{1}{\lambda + 0.087\vartheta} - \frac{0.035}{\vartheta^3 + 1} \end{cases} \tag{9}$$

The generator torque is calculated as a tabular function of the filtered generator speed, comprising five control regions: 1, 2a, 2b, and 3, as stated in the National Renewable Energy Laboratories (NREL) standard 5-MW wind turbine as shown in Fig. 3 (Jonkman, 2007).

The parametric values of the floating offshore wind turbine considered in this manuscript are presented in (Jonkman, 2007) Table 1.

3.3. Equation of motion of the hybrid FOWT-OWCs

This section provides an overview of the theory governing the hybrid model, which was created to incorporate WECs called OWCs into a large wind turbine on a floating barge platform (5 MW). Numerical tools in the frequency domain are built to examine the proposed design based on linear theory. The project's overall financial cost can be decreased by including a WEC by sharing mooring and energy infrastructure. The hybrid model was developed using MultiSurf, a geometry designer tool, and a computational diffraction-radiation code, WAMIT, an assumption of a standard well and Power-Take-Offs (PTOs) equipment turbine (Penalba et al., 2017). The entire set of time-domain nonlinear equations of motion for the 5 MW FOWT with an OWC-equipped platform can be obtained as (Jonkman, 2007):

$$M_{ij}(\xi,u,t)\ddot{\xi} = F_l(\xi,\dot{\xi}u,t) \tag{10}$$

where ξ, $\ddot{\xi}$ is the first and second time derivative of the j^{th} Degree Of Freedom (DOF), respectively. M_{ij} is the inertia mass matrix component, which depends nonlinearity on the set of system DOFs (ξ), time (t), and u

Table 1
NREL 5-MW FOWT features.

Parameter	Value
Height of Hub	90 m
Mass of center location	38.23 m
Diameter of rotor	126 m
Blades in number	3
Initial rotational speed	12.1 rpm
Mass of blades	53,220 kg
Mass of nacelle	240,000 kg
Mass of Hub	56,780 kg
Mass of tower	347,660 kg
Power output	5 MW
Cut-in, rated, and saturated wind speed	773.8 m

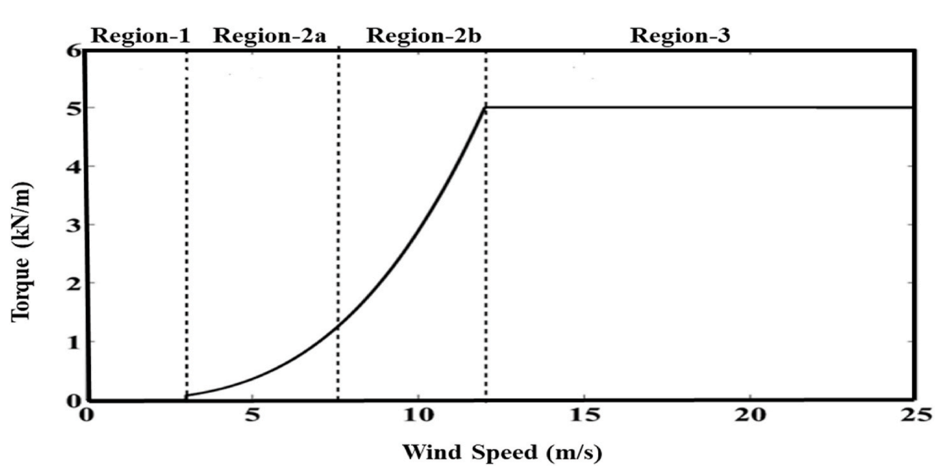

Fig. 3. Torque-versus-speed response of the variable-speed controller.

(control inputs). The term on the right side of Eq. is the generalized external force that affects the integrated system, including aerodynamic load on the blades and nacelle and hydrodynamic forces on the platform, including elastic and servo forces associated with i^{th} DOF. The ξ from Eq. (10) is defined as:

$$\xi = \begin{bmatrix} roll \\ pitch \\ yaw \\ surge \\ heave \\ sway \\ fore-aft \\ side-to-side \end{bmatrix} \tag{11}$$

The generalized system of linear equations of motion in the frequency domain can be addressed as (Aubault et al., 2011):

$$I_F(\omega)\ddot{\xi} + D_F(\omega)\dot{\xi} + C_F\xi = \widehat{F}(\omega) + \widehat{F}_{PTO}(\omega) \tag{12}$$

where $I_F(\omega)$, $D_F(\omega)$ and $C_F(\omega)$ are the inertia, damping, and stiffness matrices of the FOWT, respectively, $\widehat{F}(\omega)$ denotes the total forces caused by hydrodynamic and viscous drag of the waves, and $\widehat{F}_{PTO}(\omega)$ represents the corresponding forces from the OWCs.

$$I_F(\omega) = A_{Hyd}(\omega) + M_{pltfrm}(\omega) + M_{Twr} \tag{13}$$

$I_F(\omega)$ Includes the frequency-dependent 8×8 matrix. $A_{Hyd}(\omega)$, $M_{pltfrm}(\omega)$ and M_{Twr} represent the platform added mass, actual platform mass, and tower mass, respectively. The damping matrix can be described by Eq. (14) as follows:

$$D_F(\omega) = D_{Hyd}(\omega) + D_{Twr} + D_{Vscs} + D_{chmbr} \tag{14}$$

where $D_{Hyd}(\omega)$ and D_{Twr} are the damping matrices of floating barge platform and flexible tower. The nonlinear viscosity on the platform is denoted byD_{Vscs}. D_{chmbr} Represents the overall external damping caused by PTO's effect. The stiffness matrix from Eq. (10) can be described by Eq. (15) as:

$$C_F(\omega) = C_{Hyd}(\omega) + C_{Morng} + C_{Twr} \tag{15}$$

where the stiffness matrix $C_F(\omega)$ consists of the hydrostatic restoration matrix of the platform obtained by WAMIT$C_{Hyd}(\omega)$, the mooring lines spring stiffness coefficients C_{Morng} and the stiffness matrices of the tower C_{Twr}.

The pressure inside the chamber for the four integrated OWCs can be assumed to be uniform because the internal free surface operates like a piston. From this perspective, the OWC's impact on overall dynamics considered as an external force is expressed (M'zoughi et al., 2021) as:

$$\widehat{F}_{PTO}(\omega) = -p(\omega)S \tag{16}$$

where p the pressure drop across the turbine S is the internal free surface area; as a result of compression and decompression, air density and pressure measurements result in an isentropic transformation. If air is considered an ideal gas, the time-related air density describes the state of the chamber at rest, defined by

$$\rho = \rho_a\left(\frac{p}{p_o}\right)^{\frac{1}{\alpha}} \tag{17}$$

where α defines the heat capacity ratio of air. Linearizing the time derivative of the air density,

$$\dot{\rho} = \rho_a\left(\frac{1}{\alpha p_o}\right)\dot{p} \tag{18}$$

Then, inside the chamber, the linearized mass flow can be calculated as follows,

$$\dot{m} = \frac{d(\rho V)}{dt} = \frac{\rho_a}{\alpha p_o}\dot{p}V_o + \rho_o\dot{V} \tag{19}$$

where V is the air chamber's volume.

A Wells turbine with a diameter of D and rotational velocity N is characterized by a linear relationship between the pressure and flow coefficient using the terminology of non-dimensional turbo-machinery (Torresi et al., 2008):

$$\psi = K\zeta \tag{20}$$

The pressure and flow coefficients are defined as:

$$\psi = \frac{p}{\rho_a N^2 D^2} \tag{21}$$

$$\zeta = \frac{\dot{m}}{\rho_a N D^3} \tag{22}$$

The linear relationship can be described as follows: while considering the non-dimensional flowrate and the presumption that the pressure drop is proportional to it,

$$\psi_C = K_C\zeta_C = \frac{p}{\rho_a g H} \tag{23}$$

$$\zeta_C = \frac{2\pi\dot{m}}{\rho_a\omega S H} \tag{24}$$

where g is the acceleration gravity. Hence, following these equations, the mass flow within the turbine can be expressed by:

$$\dot{m}(\omega) = \frac{S\omega p}{2\pi g K_c} \tag{25}$$

After combining Eq. (19) and Eq. (25), the pressure with complex amplitude can be shown in the frequency domain as:

$$\widehat{p}(\omega) = i\omega\frac{\Upsilon}{S\omega\left[1+(\varepsilon\Upsilon)^2\right]}\widehat{V} - \omega^2\frac{\varepsilon\Upsilon^2}{S\omega\left[1+(\varepsilon\Upsilon)^2\right]}\widehat{V} \tag{26}$$

where $\widehat{V}$ is the complex amplitude of the oscillation in air volume, and Υ andε are the constants specified by:

$$\Upsilon = 2\pi\rho_a g K_C \tag{27}$$

$$\varepsilon = \frac{V_a}{\Upsilon\rho_a S} \tag{28}$$

The total PTO force can be rewritten by combining Eq. (16) and Eq. (26).

$$\widehat{F}_{PTO}(\omega) = i\omega B_{PTO}\widehat{x}_r + \omega^2 K_{PTO}\widehat{x}_r \tag{29}$$

where $\widehat{x}_r$ is the complex relative displacement amplitude. According to Eq. (30), the linear load imposed by the PTO comprises a dissipative term proportional to the relative velocity and a reactive term forced on by the chamber's compressed air and corresponding to relative acceleration. The dissipative term becomes proportional to the volume variation, and the reactive term becomes proportional to the rate of volume change when the damping, B_{PTO} and spring, K_{PTO} coefficients are divided by the area of the internal free surface, S. The PTO damping and spring coefficients are derived from Eq. (26), respectively.

$$B_{PTO}(\omega) = \frac{\Upsilon}{\omega\left[1+(\varepsilon\Upsilon)^2\right]} \tag{30}$$

$$K_{PTO}(\omega) = \frac{\varepsilon\Upsilon^2}{\omega^2\left[1+(\varepsilon\Upsilon)^2\right]} \tag{31}$$

Finally, the following results have been derived for the system's frequency-dominant equations of motion for the 8-DOFs FOWT:

$$I_F(\omega)\widehat{\ddot{\xi}} + (D_F(\omega) + B_{PTO}(\omega))\widehat{\dot{\xi}} + (C_F + K_{PTO}(\omega))\widehat{\xi} = \widehat{F}(\omega) \tag{32}$$

4. Proposed hybrid FOWT-OWCs model

4.1. Platform geometry design

For active structural control, four OWCs have been integrated into 5 MW FOWT. The initial stage is to design the geometry for the hybrid system. The geometry of the proposed platform was created using MultiSurf, a robust and computational module that allows the creation of 3D models of hybrid systems and their individual components. The software will enable us to design a wide range of marine platforms, including hulls, decks, keels, interiors, superstructures, free-form curves, and surfaces.

Both platform pitch and tower top displacement oscillations rise significantly when exposed to high wind speeds and wave elevations. Various platform configurations (M'zoughi et al., 2021; Aboutalebi et al., 2021), open-moonpools, and standard barge platforms have been tested, as shown in Figs. 4 and 5. In order to make use of the buoyant geometric model, the WAMIT tool must be connected to MultiSurf so as to calculate hydrodynamic loads caused by water pressure on wet surfaces. The corresponding panel method geometries are shown in Figs. 4 and 5 (Guo et al., 2016).

Two potential representative platforms have been examined in this study to reflect specific unique characteristics. Fig. 3 illustrates the first platform, a standard barge type within a quarter of the body. The second platform shown in Fig. 4 is a barge platform with four corners OWCs and half-open moonpools. The third platform, which is a barge platform with four corners OWCs containing fully open moonpools, is depicted in Fig. 5. Each OWC is 5m × 5m x 10 m in size, meshed with 8960, 9940, and 9840 rectangular panels, and is positioned 1m from the sidewalls. The information of the barge platform and the four identical OWCs are shown in Table 2. The mass, including ballast, of the floating platform, is 7,466,330 kg. This mass was determined to be the sum of the weights of the rotor-nacelle assembly, tower, platform, and mooring system (excluding the little portion that rests on the seafloor) in water. The mass, including ballast, is comparable to other wind-floating structures. For instance, in (Xu and Day, 2021). Xu et *al.* study, the total combined platform mass, including ballast for a spar-type offshore floating wind turbine is 7,500,000 kg.

4.2. Advanced hydrostatic and hydrodynamic computations

It is essential to adequately consider the hydrodynamic and hydrostatic metrics when developing the geometry of the aforementioned proposed four OWCs-based barge platforms. Therefore, the intricate computations of these attributes have been carried out using the WAMIT numerical tool. For the linear analysis of surface wave interactions with various floating and submerged object types, the WAMIT diffraction panel program was designed. Hydrostatic and hydrodynamic coefficients were calculated using the MultiSurf file directly in diffraction radiation WAMIT to create the matrices A_{Hyd} , B_{Hyd}, and C_{Hyd}. In terms of the suitable pairings of the water density ρ, gravity acceleration g, incident-wave amplitude A, frequency ω, and length scale L. The Gauss divergence theorem can represent all hydrostatic data as surface integrals over the mean body wetted surface S_b. WAMIT allows the evaluation of all three volume forms under the assumption that the coordinates of the center of buoyancy are set to zero.

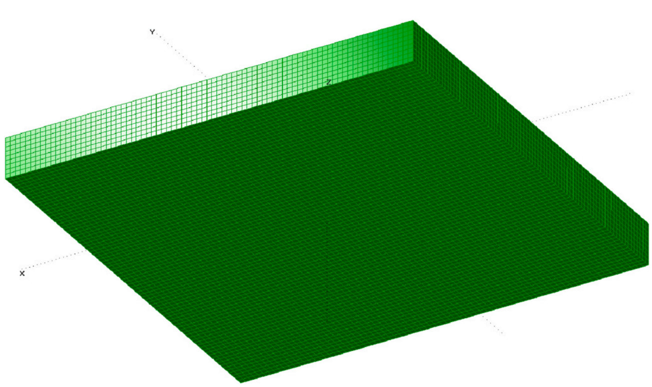

Fig. 4. Standard Barge Platform WAMIT panels.

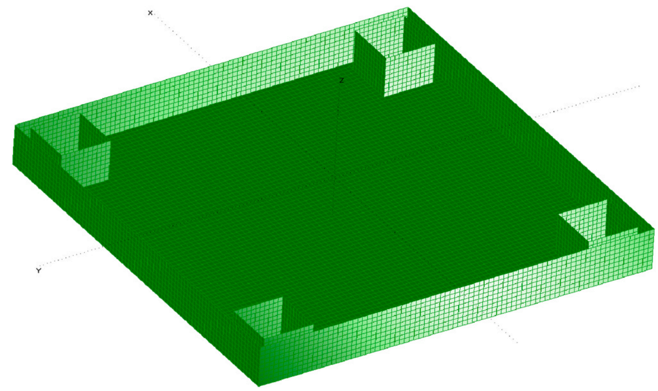

Fig. 5. Standard barge platform with 4 open MoonPools WAMIT panels.

Table 2
Standard barge and the four OWCs-based barge platforms' features (Jonkman, 2007).

Parameter	Value
Size of platforms (W, L, and H)	40 m × 40 m × 10 m
Size of each OWC (W, L, and H)	5 m × 5 m × 10 m
Free board for both platforms for drafts	4 m, 6 m
The simple barge's water displacement	6400 m^3
Barge's water displacement when equipped with OWCs	6000 m^3
Mass, Including Ballast	7,466,330 kg
Location of CM below SWL	0.28768 m
Roll Inertia regarding CM	726,900,000 $kg \cdot m^2$
Pitch Inertia regarding CM	726,900,000 $kg \cdot m^2$
Yaw Inertia regarding CM	1,453,900,000 $kg \cdot m^2$
Anchor (Water) Depth	150 m
Distancing of Opposing Anchors	773.8 m
Unstretched Line Length	473.3 m
Length of Neutral Line Resting on Seabed	250 m
Line Diameter	0.0809 m
Density of Lines	130.4 $kg/\ m$
Line Extensional Stiffness	589,000,000 N

$$\forall = -\iint xn_1 dS = -\iint yn_2 dS = -\iint zn_3 dS \tag{33}$$

and the center of buoyancy parameters:

$$x_b = \frac{-1}{2\forall}\iint_{S_b} n_1 x^2 dS \tag{34}$$

$$y_b = \frac{-1}{2\forall}\iint_{S_b} n_2 x^2 dS \tag{35}$$

$$z_b = \frac{-1}{2\forall}\iint_{S_b} n_3 x^2 dS \tag{36}$$

The hydrostatic and gravitational restoring coefficients can be determined by a matrix concerning their coordinates.

$$C_{Hyd} = \begin{bmatrix} 0 & 0 & 0 & 0 & 0 & 0 \\ 0 & 0 & 0 & 0 & 0 & 0 \\ 0 & 0 & a_{33} & a_{34} & a_{35} & 0 \\ 0 & 0 & 0 & a_{44} & a_{45} & a_{46} \\ 0 & 0 & 0 & 0 & a_{55} & a_{56} \\ 0 & 0 & 0 & 0 & 0 & 0 \end{bmatrix} \tag{37}$$

The matrix elements are given by,

$$a_{3,3} = \rho g \iint_{S_b} n_3 dS, a_{3,4} = \rho g \iint_{S_b} y n_3 dS \quad a_{3,5} = -\rho g \iint_{S_b} x n_3 dS$$

$$a_{4,4} = \rho g \iint_{S_b} y^2 n_3 dS \rho g \forall z_b - mgz_g, a_{4,5} = -\rho g \iint_{S_b} xyn_3 dS \iint$$

$$a_{4,6} = -\rho g \forall x_b + mgx_g \quad a_{5,5} = \rho g \iint_{S_b} x^2 n_3 dS + \rho g \forall z_b - mgz_g$$

$$a_{5,6} = -\rho g \forall y_b + mgy_g$$

where m is the body mass andx_g, y_g and z_g are the center of gravity coordinates. Finally, the following equations describe the added mass and damping coefficients.

$$A_{ij} - \frac{iB_{ij}}{\omega} = \rho \iint_{S_b} n_i \varphi_j dS \tag{38}$$

In order to integrate the hydrodynamic information and additional masses into OpenFAST, WAMIT is used. Fig. 6 above describes the method for integrating modules to create the aero-hydro-servo-elastic simulation.

4.3. ANN-based hybrid FOWT-OWCs model

ANN can learn from data to estimate the corresponding output since it can identify patterns and make decisions based on real recorded data.

ANNs are particularly associated with weighted signals a_{jk} in the input, output, and hidden layers. The neurons are composed of an activation functionσ_j, a bias function b_J, and a weighted sum function x_j can be defined as follows (Liu et al., 2022):

$$x_j = \sum_{k=1}^{N} a_{jk} z_k + b_j \tag{39}$$

The desired ANN used in this work is a feed-forward network with three featured input layers: wave elevation, wind speed, and throttle (ranging from 0 to 90°). The network has 3 hidden layers, each containing 10 fully connected neurons and an output layer with 2 neurons for the estimation of the tower fore-aft displacement and platform pitch. The best-chosen method is used to find the number of hidden layers/neurons in such a complex process and challenging operation. The technique starts from a few latent layers or neurons that multiply. Each time a new network structure is trained, this cycle is repeated to obtain a minimum MSE. Various learning rate hyperparameters of 0.01, 0.001, and 0.0001 have been considered, with batch sizes 32, 64, and 128, and different hidden layers with different sets of neurons. Finally, the learning rate of 0.001 with a batch size of 32 and 3 hidden layers with neurons provides promising results.

$$\sigma_j(x_j) = \left\{ \begin{array}{ll} \max(0, x_j) & \text{ReLU} \\ \dfrac{1}{(1 + e^{-x_j})} & \text{Sigmoid} \\ \dfrac{(e^{x_j} - e^{-x_j})}{(e^{x_j} + e^{-x_j})} & \text{Tangent} \end{array} \right\} \tag{40}$$

A wide range of activation functions has been investigated to train the network. The Rectified Linear Unit (ReLU) activation function has

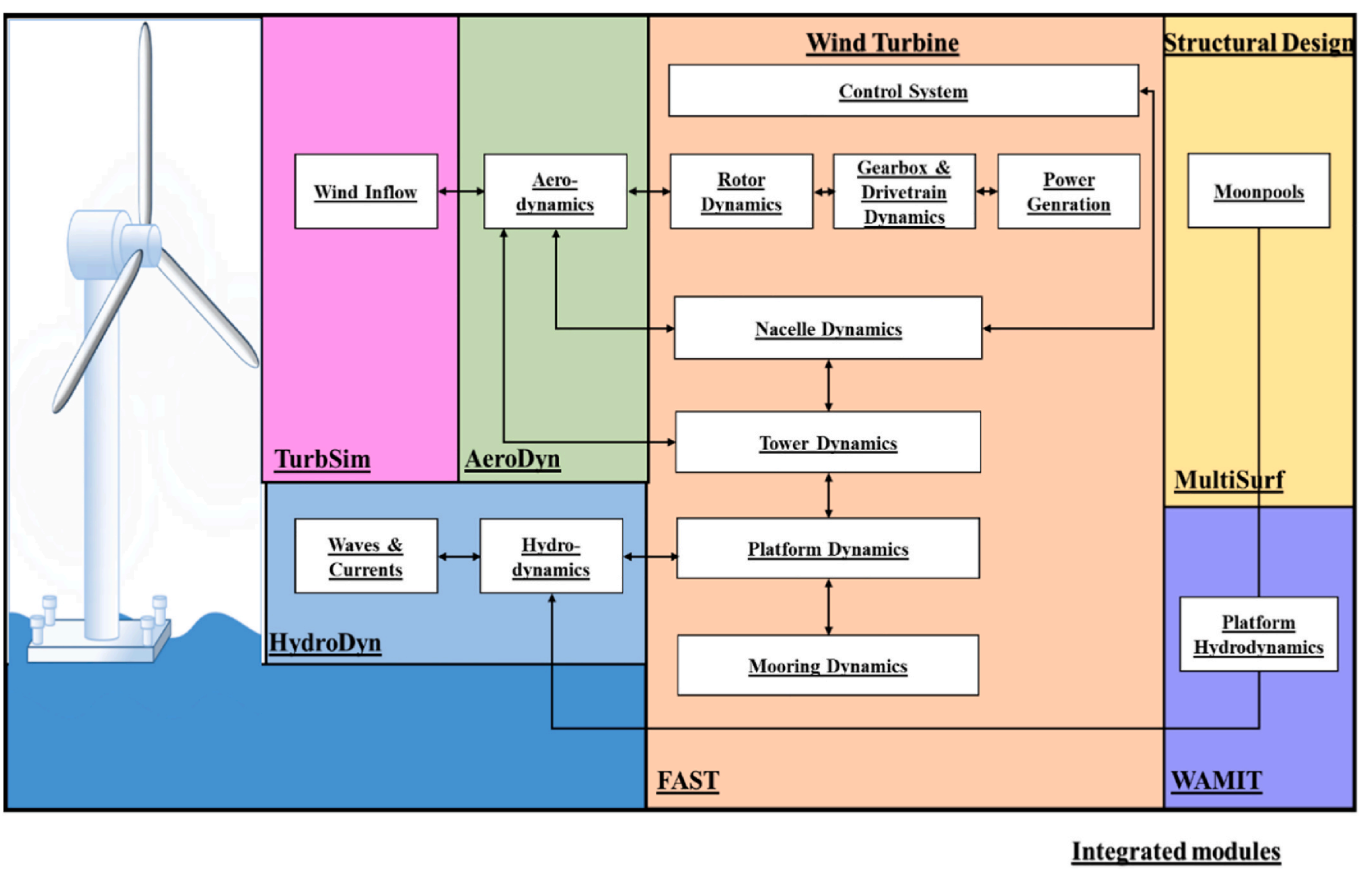

Fig. 6. Integrating key modules to simulate aero-hydro-servo-elastic dynamics.

been applied to the input layer, and the hyperbolic tangent activation function has been used to the hidden layers. Nevertheless, Single hidden layer networks, sometimes called Vanilla Neural Networks, perform poorly in extremely complex and nonlinear situations. On the other hand, deep neural networks are network topologies with multiple hidden layers that perform better. Therefore, due to the proposed barge FOWT system's complexity, Multi-Layer Perceptron (MLP) has been adopted, as illustrated in Fig. 7.

The MSE has been calculated to select the best candidate for the proposed hybrid system.

$$MSE = \frac{1}{n}\sum_{k}^{n}\left(o_k - o_k^{'}\right)^2 \tag{41}$$

where n represents the number of observations, o_k is the target output, and $o_k^{'}$ is the ANN's estimated outcome.

Hessian for the Newton-Raphson (Lindh et al., 1995) is:

$$H_s = J^T J \tag{42}$$

and the gradient error represents the first derivative of the network error with respect to weights and biases, and can be computed using the Jacobian as follows:

$$s = J^T E \tag{43}$$

$$J(a) = \begin{pmatrix} \frac{\partial E_1(W_a)}{\partial W_a} & \frac{\partial E_1(W_a)}{\partial W_a} \cdots \frac{\partial E_1(W_a)}{\partial W_a} \\ \frac{\partial E_2(W_a)}{\partial W_a} & \frac{\partial E_2(W_a)}{\partial W_a} \cdots \frac{\partial E_2(W_a)}{\partial W_a} \\ \vdots \vdots \ddots \vdots & \\ \frac{\partial E_n(W_a)}{\partial W_a} & \frac{\partial E_n(W_a)}{\partial W_a} \cdots \frac{\partial E_n(W_a)}{\partial W_a} \end{pmatrix} \tag{44}$$

where W_a is the weight vector and E is the error between the target and estimated outputs.

The LMA algorithm is employed because it improves the convergence rate by considering both curvature and slope. As a result, it employs modified gradient descent with a weight-updating equation (Wilson and Martinez, 2003):

$$W_{a_{k+1}} = W_{a_k} - [H_s + \mu I]^{-1} J^T E \tag{45}$$

where μ and I are learning rate and identity matrix.

Finally, gradient performance is as:

$$\nabla f(W_a) = 2J^T(W_a).E(W_a) \tag{46}$$

The dynamics of the hybrid system were derived using OpenFAST after introducing varied wind speeds and wave elevations that have been taken into account to obtain outputs. After that, the proposed ANN algorithm, which resembles the behavior of nonlinear OpenFAST, was used to generate the estimated model, as shown in Fig. 8.

5. Proposed fuzzy approach

There are two main tasks within the fuzzification stage: first, the control variables are read, measured, and scaled; and then, the resulting numeric values are mapped into subsequent linguistic variables that compose the fuzzy variables with appropriate membership values.

The depth of knowledge module includes the fundamental rules that define the control objectives by linguistic variables as well as the fuzzy membership functions provided for each control variable. The inferences module must be able to control fuzzy logic-based control behaviors and imitate human decision-making. The defuzzification module converts the linguistic decision variable to a numerical one.

High wind speeds, platform pitch, and tower top displacement significantly increase, as demonstrated using OpenFAST on various platform moonpool configurations, open-moonpools, closed moonpools, and standard barge platforms, as shown in Figs. 4 and 5. Moreover, the open-moonpool simulations have less amplitude than standard barge platforms, and therefore, OWCs can be used as structural control in a less windy environment. However, at high speeds, hybrid platform oscillations increase, causing the system to destabilize, as shown in Fig. 9. Therefore, the ideal behavior of the hybrid platform would be to behave like an open-OWCs barge platform for platform pitch between 0 and 3 deg and act like a closed-OWCs-barge platform after 3 deg. As a result, the proposed control strategy aims to control the OWC air valve using a fuzzy controller, as illustrated in Fig. 10, with defined surfaces in Fig. 11. This is accomplished by measuring the platform pitch and establishing a feedback loop to control the valves. It has been ascertained that when the platform pitch is increased, the actuator valve should be closed accordingly.

The inputs to the fuzzy controller are the platform's pitch $|\theta\mathrm{P}|$ and time derivative $|d\theta\mathrm{P}|$; the platform's velocity determines the state of the valve's opening based on the platform's pitch. The membership

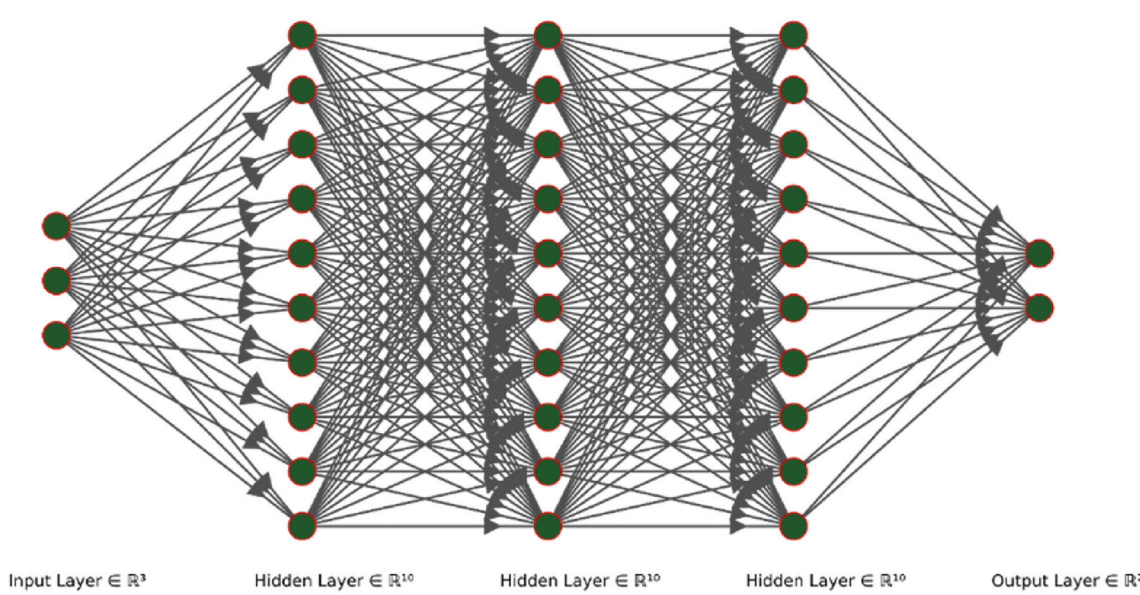

Fig. 7. Proposed multi-layer perceptron network.

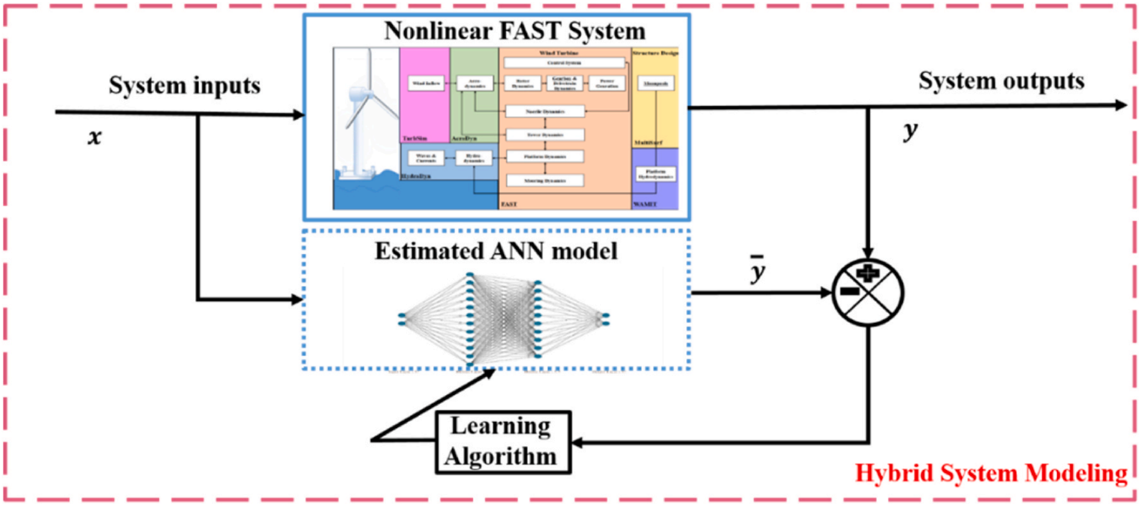

Fig. 8. Proposed ANN-based FOWT-OWCs hybrid system model using OpenFAST data.

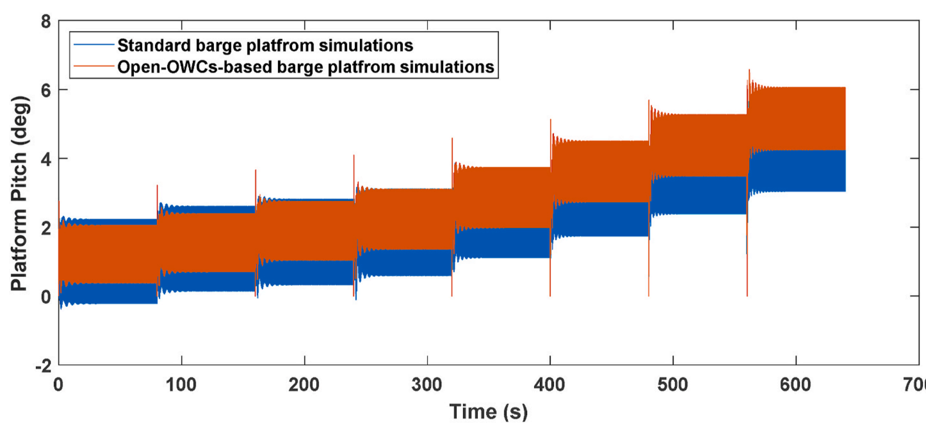

Fig. 9. Closed-OWC-based Barge Platform and Open-OWCs-based Barge Platform simulations.

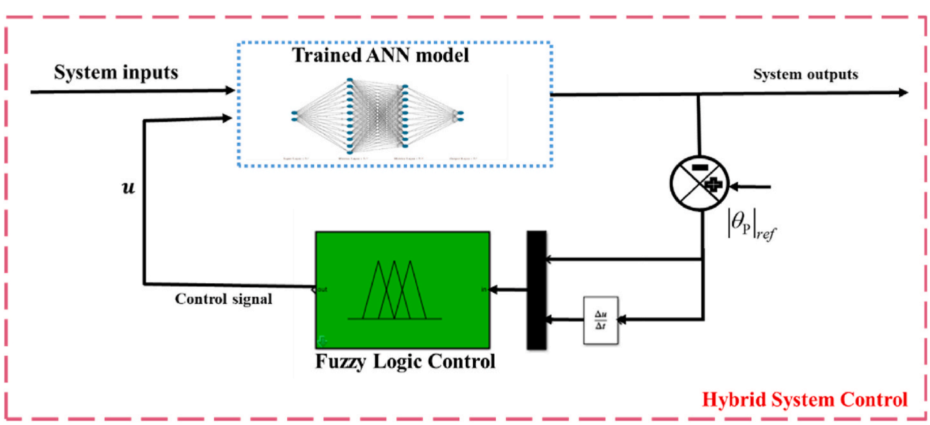

Fig. 10. Proposed FLC-based collective airflow control for OWC valves in the hybrid platform.

functions depicted in Figs. 12–14 describe the fuzzy sets *Ai* and *Bi*. Gaussian and triangular membership functions were employed as the linguistic variables for the input and output. The linguistic levels for the inputs are Very Small (*VS*), Small (S), Medium (M), Large (L), and Very Large (VL). The linguistic levels for the output throttle valve are Close Fast (CF), Close Slow (CS), Close (C), Open Slow (OS), and Open Fast (OF).

The following relationships have been validated by the membership functions shown in Eq. (47).

$$A = \sum_{i}^{n} \mu_A \frac{(x_i)}{x_i} \Rightarrow \{(x, \mu_A(x))\} \quad x \in X \tag{47}$$

The grade of the membership function for the output according to the Gaussian perspective:

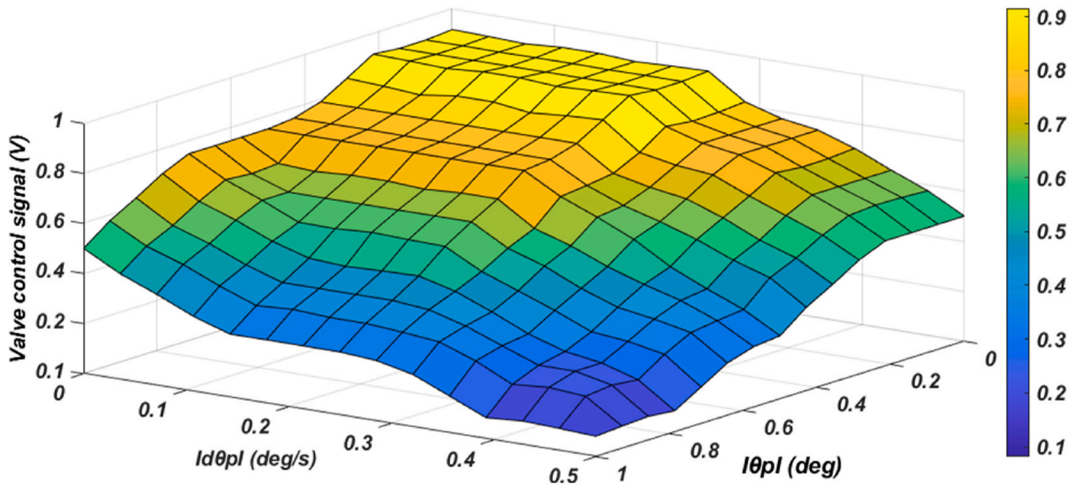

Fig. 11. Fuzzy surface of valve control signal (V) against platform pitch $|\theta_P|$ and platform rotational speed $|d\theta_P|$.

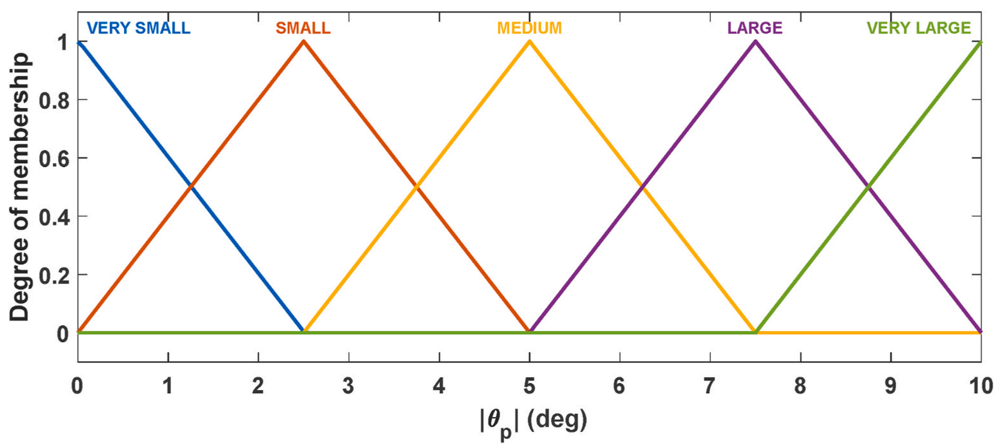

Fig. 12. Membership functions for input $|\theta_P|$

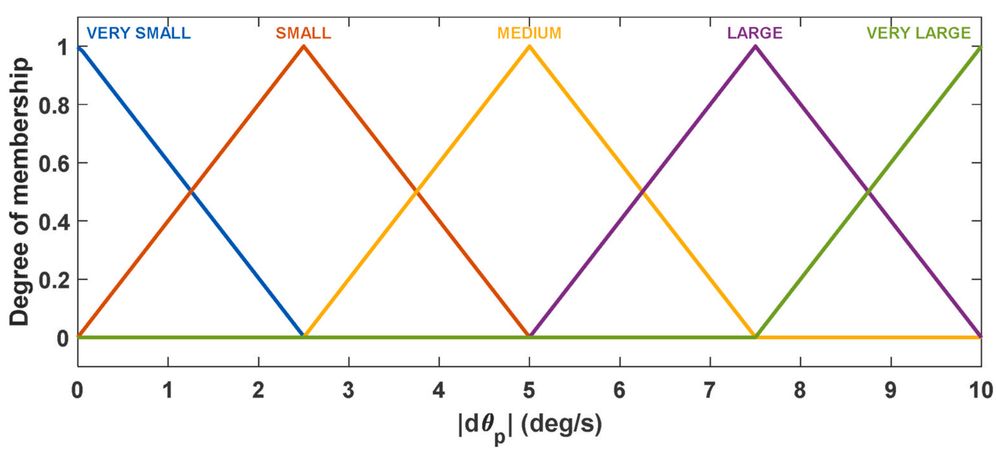

Fig. 13. Membership functions for input $|d\theta_P|$

$$gassian(x; c, \sigma) = e^{-\frac{1}{2}\left(\frac{x-c}{\sigma}\right)^2} \tag{48}$$

$$g_{CF}(x) = e^{-\frac{1}{2}\left(\frac{x}{\sigma}\right)^2} \tag{49}$$

$$g_{CS}(x) = e^{-\frac{1}{2}\left(\frac{x-2.5}{\sigma}\right)^2} \tag{50}$$

$$g_{C}(x) = e^{-\frac{1}{2}\left(\frac{x-5}{\sigma}\right)^2} \tag{51}$$

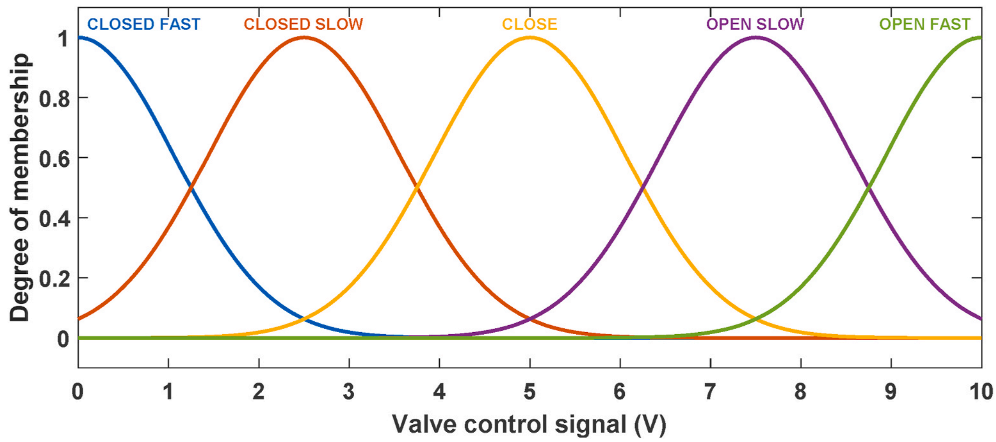

Fig. 14. Membership functions for output valve.

$$g_{OF}(x) = e^{-\frac{1}{2}\left(\frac{x-7.5}{\sigma}\right)^2} \tag{52}$$

$$g_{O}(x) = e^{-\frac{1}{2}\left(\frac{x-10}{\sigma}\right)^2} \tag{53}$$

$$\left\{\begin{array}{l} \mu_{VS}(x) = \left\{\begin{array}{ll} 0 & x < 0 \\ \dfrac{2.5-x}{2.5} & 0 \le x \le 2.5 \\ 0 & x > 0 \end{array}\right\} \\ \mu_{S}(x) = \left\{\begin{array}{ll} 0 & x < 0 \\ \dfrac{2}{5}x & 0 \le x \le 2.5 \\ -\dfrac{2}{5}x + 2 & 2.5 \le x \le 5 \\ 0 & x > 5 \end{array}\right\} \end{array}\right.$$

$$\left\{\begin{array}{l} \mu_{M}(x) = \left\{\begin{array}{ll} 0 & x < 0 \\ \dfrac{x-2.5}{2.5} & 2.5 \le x \le 5 \\ \dfrac{7.5-x}{2.5} & 5 \le x \le 7.5 \\ 0 & x > 7.5 \end{array}\right\} \\ \mu_{L}(x) = \left\{\begin{array}{ll} 0 & x < 5 \\ \dfrac{x-5}{2.5} & 5 \le x \le 7.5 \\ \dfrac{10-x}{2.5} & 7.5 \le x \le 10 \\ 0 & x > 10 \end{array}\right\} \end{array}\right. \tag{54}$$

$$\left\{ \mu_{VL}(x) = \left\{\begin{array}{ll} 0 & x < 7.5 \\ \dfrac{x-7.5}{2.5} & 7.5 \le x \le 10 \\ 0 & x > 10 \end{array}\right. \right\}$$

where $\mu(x)$ is the vector of inputs. There were two sets of 25 rules considered, as shown in Table 3. The idea is that as the platform pitch increases, the actuator valve should close accordingly.

6. Model validation and control results

This section describes the simulations that were carried out to evaluate the effectiveness of the proposed method of modeling and control of the hybrid FOWT-OWCs system. The framework for collecting, simulating, and developing the network is shown in the flow diagram in Fig. 15. As shown in the flow chart, six steps are employed to establish the hybrid framework's modeling and control. Step 1: Geometry design. MultiSurf is used to define the structural geometry of the platform. Step 2: Forces calculation: The hydrodynamic forces, added masses, damping coefficient, and hydrostatic matrices are calculated using WAMIT. Step 3: Structure dynamics and datasets collection: The data obtained from MultiSurf and WAMIT is fed to OpenFAST. Then, simulations of the hybrid platform were carried out using the OpenFAST NREL 5 MW tool to get the dynamics to determine system behavior. After the OpenFAST simulation, the datasets for the proposed computation machine-learning algorithm are collected. Step 4: Model training and establishment: An ANN model has been developed after data processing, considering the lowest MSE. Step 5: Control development: Finally, a Fuzzy Logic Controller is used to regulate the platform's pitch and fore-aft movement to stabilize the system.

6.1. ANN model validation

In order to obtain the best MSE, several configurations have been tested with different hidden layers and neurons in the feed-forward approach. The three inputs considered in this study are the wind

Table 3
Proposed Fuzzy rules.

$\lvert d\theta P\rvert$ $\lvert\theta P\rvert$	*VS*	*S*	*M*	*L*	*VL*
VS	*OF*	*OF*	*OS*	*OS*	*C*
S	*OF*	*OF*	*OS*	*C*	*CS*
M	*OF*	*OF*	*OS*	*C*	*CS*
L	*OS*	*OS*	*C*	*CS*	*CF*
VL	*C*	*C*	*CS*	*CF*	*CF*

The grade of the membership function for FLC inputs are.

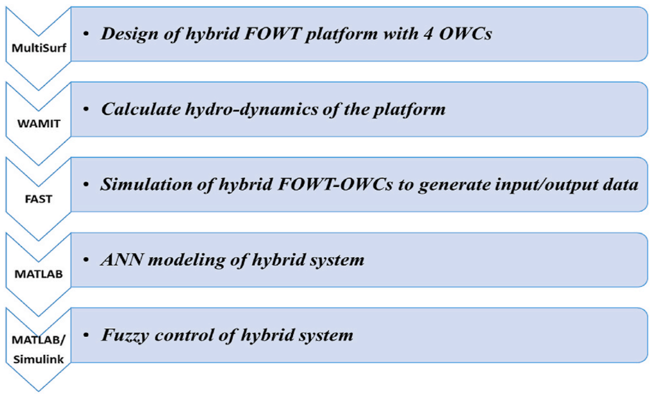

Fig. 15. Flow chart for modeling and control of the Hybrid system.

speed, which increases from 8 m/s to 15 m/s, and the wave elevation and valve position, which vary from 0 to 90°, as shown in Figs. 16–18. To avoid transients, the first 500 simulations have been omitted.

$$v(t) = \begin{Bmatrix} 8\,m/s & t_1 < t < t_2 \\ 9\,m/s & t_2 < t < t_3 \\ . & \\ . & \\ . & \\ 15\,m/s & t_{15} < t < t_n \end{Bmatrix} \tag{55}$$

where t_1 to t_n is the time span from 1s to 700s.

A linear activation function (ReLU) in the output layer and a sigmoid activation function for the neurons in each hidden level of the ANN model's five hidden layers. 70% of the data were used for training, 15% were used for validation, and 15% have been used for testing. Multi-layered can perform linear and nonlinear computing and an extremely well approximation of any logical functions. The proposed ANN's training, testing, and validation graphs are shown in Fig. 19 and Table 4. The blue lines are for training, the green curves are for validation, and the red curves are for testing. As shown in Fig. 8, the best validation performance in the training history was obtained for MSE = 0.13 at 7 epochs. The training process has been performed on computers equipped with an Intel 8700 Six-Core processor, integrated Intel UHD Graphics 630, and an external Nvidia RTX 4000 graphics card.

The developed model (blue lines) and ANN model are represented in red lines. Figs. 20 and 21 depict the platform pitch angle and fore-aft displacement, respectively. In Table 4, it can also be seen that the regression values (***R***) are close to 1. They demonstrate that the model has been adequately trained and replicates the dynamic behavior obtained from the OpenFAST model.

As it is shown in Figs. 20 and 21, the suggested ANN model offers similar behavior to the nonlinear OpenFAST model under different scenarios. As a result, it is established that the hybrid platform ANN models are an adequate substitute.

Figs. 22 and 23 demonstrate the error signals for platform pitch and top tower fore-aft-displacemrnts, which show almost 90% accuracy of the proposed model.

6.2. *Fuzzy control of hybrid FOWT-OWCs system*

FLC has the advantage of being able to resolve nonlinear dynamics without requiring prior knowledge of the parameters of a mathematical model. At the top of the capture, chamber air valves connect to the turbine duct. This OWC modeling and control has been thoroughly researched by the authors based on the experimental data of the Mutriko OWC plant (Folley, 2016). The valve separates the air and pressure in the chamber from the pressure and air in the capture chamber, controlling the amount of airflow input. An actuator controls the valve by rotating the valve plate to the desired angular position and then holding it in place with an electromagnetic brake. In this hybrid platform, the degree of opening of the valve plate may be used to control the platform pitch.

The proposed FLC has been implemented for reduced platform pitch angular and tower displacement. The idea is actuator valve ought to close appropriately as the platform pitch increases. Based on the observed data of the structures, as shown in Fig. 9, the ideal behavior of the hybrid platform would be to behave like an open-OWCs-based barge platform for platform pitch between 0 and 3° and act like a closed-OWCs-based Barge platform after 3°, as shown in Fig. 24.

The opening and closing valves of the OWCs governor by FLC help to stabilize the platform by relying on the counterforces induced by the built-up pressure within the OWC air chambers to reduce the undesired platform pitch motion and the tower top fore-aft displacement mode (see Fig. 25). It is important to note that the fuzzy control for platform stabilization performs adequately under challenging circumstances. A comprehensive statistical analysis has been carried out and summarized in two tables. In this sense, it can be more clearly seen from Tables 5 and 6, which detailed that the vibrations are significantly reduced when the proposed controller is applied. In particular, the results presented in the tables jointly with Figs. 26 and 28 demonstrate that the fuzzy control reduces the platform pitch and tower displacement in high wind scenarios. As an example, it may be observed in Table 6 the platform pitch oscillations are reduced up to an average value of 36.75% at all wind speeds (see Fig. 27).

This work will be expanded in the future to incorporate advanced machine learning control algorithms with a feedback loop to reduce unwanted platform motion. In addition, this work will be expanded to

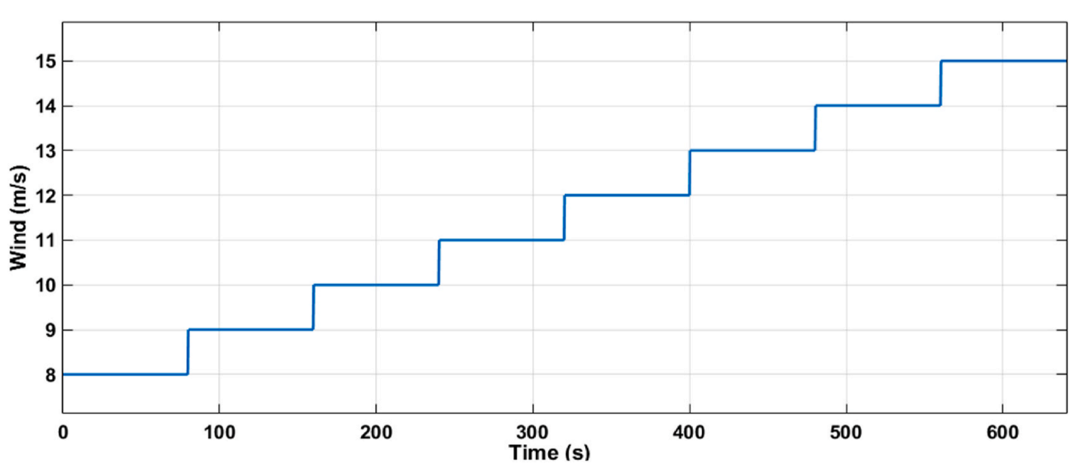

Fig. 16. Varies wind speed.

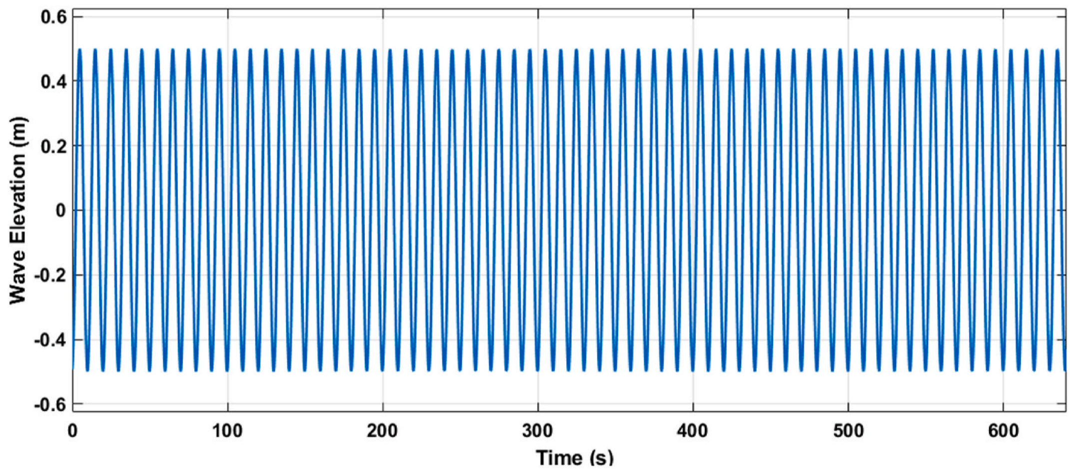

Fig. 17. Wave Elevations with amplitude, A = 1m, and 10s of the period.

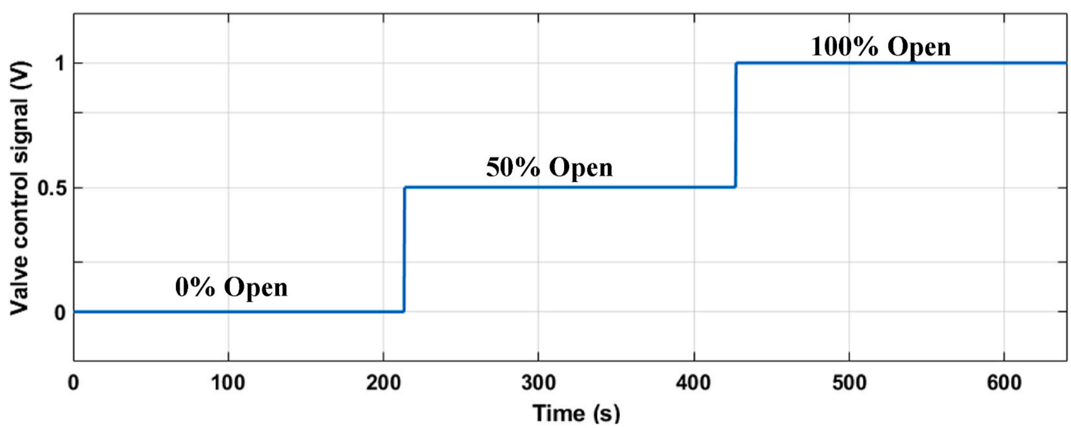

Fig. 18. Valve Position 0%, 50%, and 100% open.

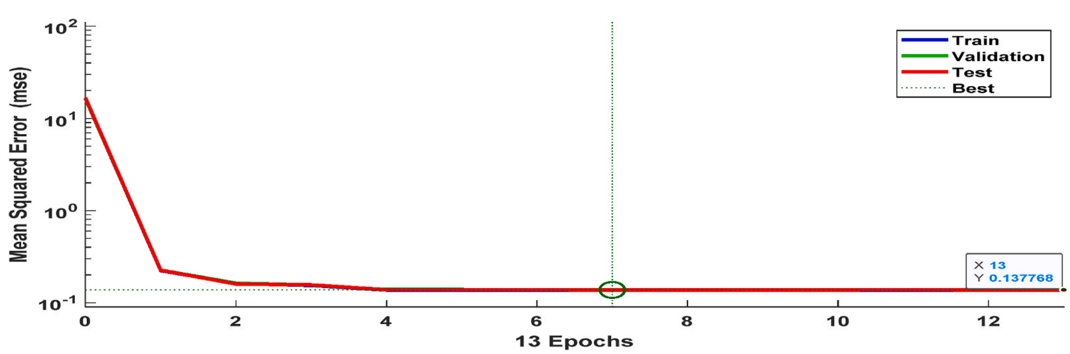

Fig. 19. Proposed ANN's performance.

Table 4
Performance, observation, and regression values.

Performance	Observations	MSE	R
Training	16,650	0.13001	0.9991
Validation	2425	0.13002	0.9991
Test	2425	0.13001	0.9922

include uncertainties and irregular waves for robust modeling and control of hybrid systems.

7. Conclusions

This article focuses on two primary objectives. Firstly, oscillating water columns have been integrated into the ITI Energy barge platform of a floating offshore wind turbine for active structure control, modeling the resulting complex hybrid system employing machine learning ANN algorithms. To do so, representative datasets have been collected by incorporating the OpenFAST hydrodynamics, aerodynamics, and servo-dynamical characteristics. These data have been then used to train an

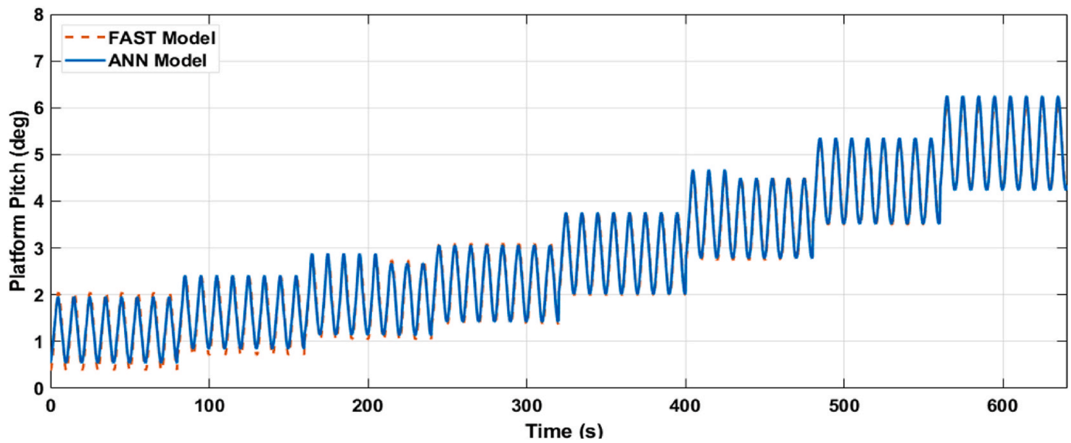

Fig. 20. Platforms Pitch with open and close valves.

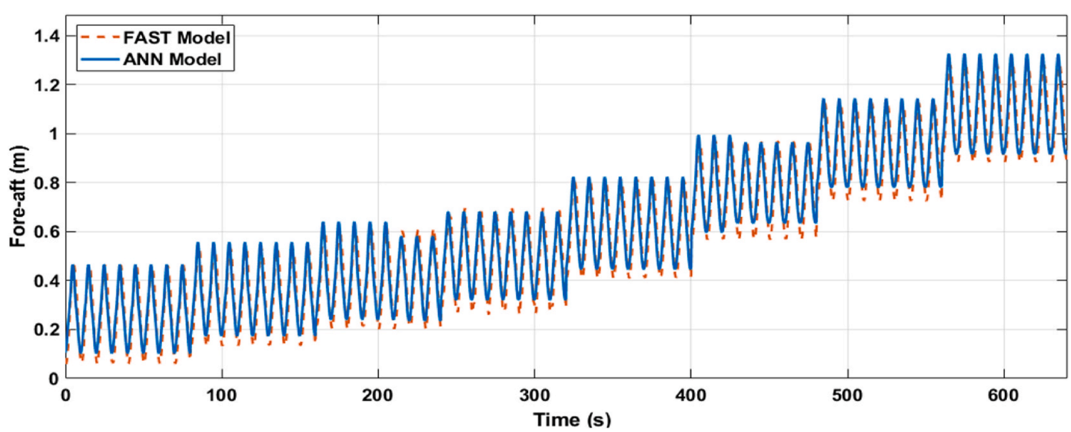

Fig. 21. Top tower fore-aft displacement with open and closed valves.

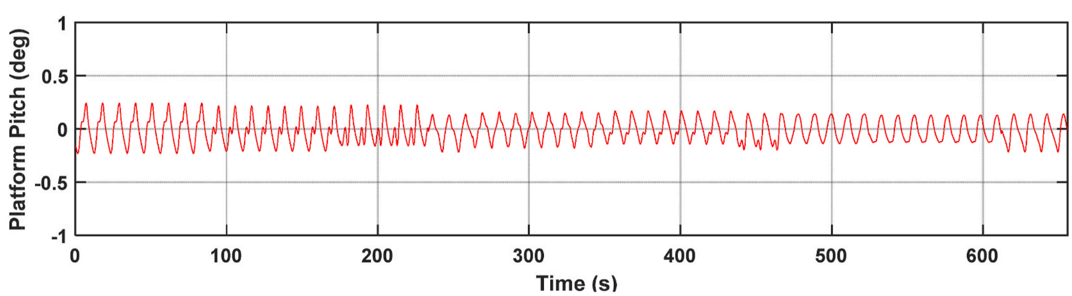

Fig. 22. Platform Pitch error.

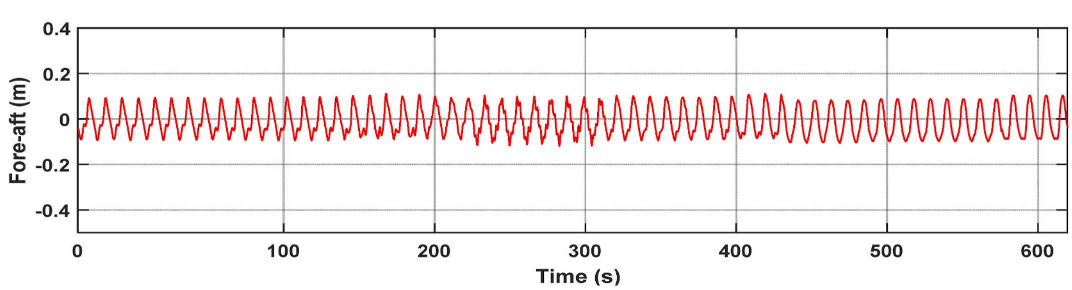

Fig. 23. Top tower fore-aft displacement error.

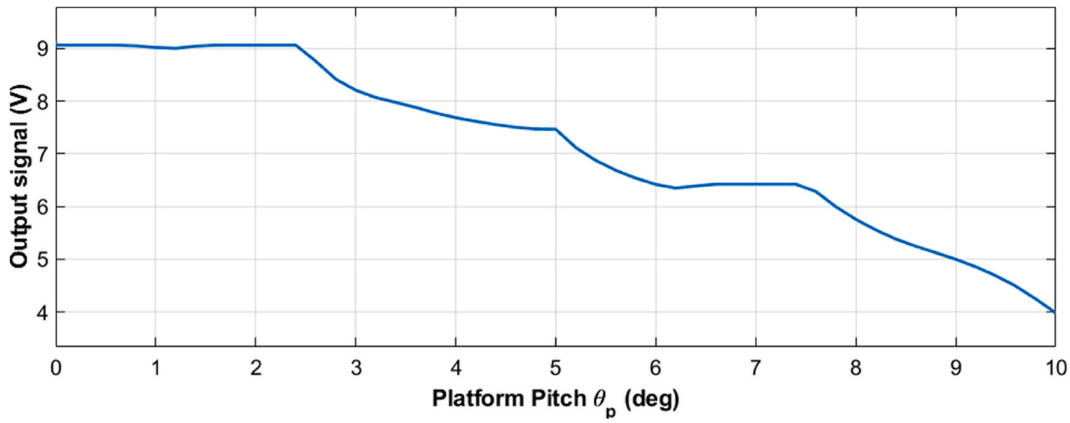

Fig. 24. Fuzzy controlled signal.

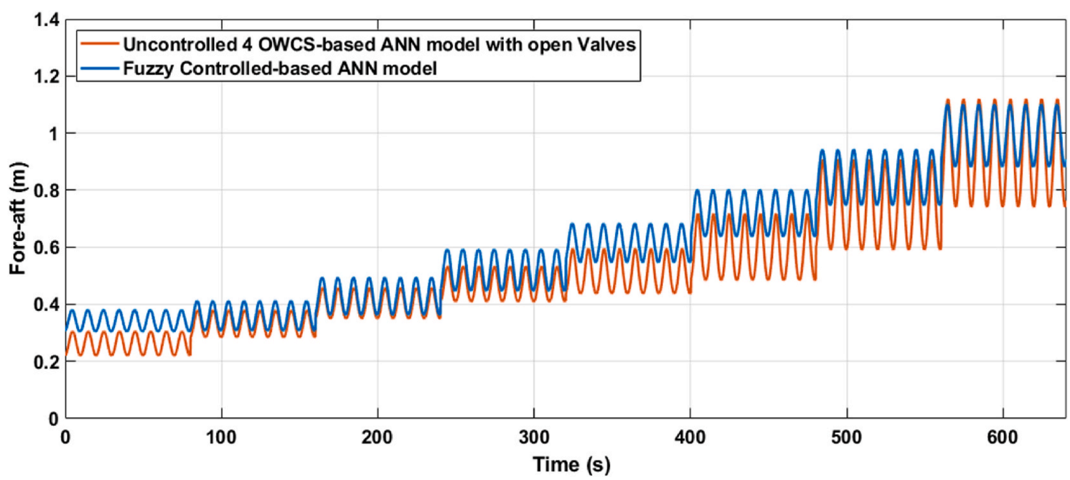

Fig. 25. Tower fore-aft displacement with FLC versus uncontrolled open valves.

Table 5
Statistical platform for fore-aft displacement analysis.

Wind Speed (m/s)	Averages/Fluctuations (m)	Control			Improvements	
		Uncontrolled with 4 closed Valves (m)	Uncontrolled with 4 open Valves (m)	Fuzzy Logic Control (m)	FLC vs.Closed-valves (%)	FLC vs.Open-valves (%)
8	*avg*	0.3420	0.9303	0.3415	11.84	11
	δ	0.0760	0.3792	0.08550		
9	*avg*	0.3595	0.7489	0.3800	8.57	0
	δ	0.1050	0.3175	0.1140		
10	*avg*	0.4280	0.5975	0.4590	3.03	0
	δ	0.1320	0.2279	0.1360		
11	*avg*	0.5190	0.5160	0.5555	7.53	0
	δ	0.1460	0.1581	0.1570		
12	*avg*	0.6145	0.4712	0.6665	29.19	13.14
	δ	0.1370	0.1244	0.1770		
13	*avg*	0.7190	0.4037	0.7875	10.84	27.16
	δ	0.1660	0.1081	0.1840		
14	*avg*	0.8440	0.3316	0.9250	6.1	38.26
	δ	0.1960	0.0955	0.2080		
15	*avg*	0.9910	0.2627	0.0681	0	41.98
	δ	0.2200	0.0857	0.2181		

ANN-based control-oriented scheme to model the behavior of the hybrid FOWT-OWCs structure.

The proposed control-oriented model has been tested for various wind speeds and wave scenarios. In order to demonstrate its computational efficiency, validity, and accuracy, the obtained ANN-based FOWT models' outputs have been compared to those of the widely accepted nonlinear complex OpenFAST model. A fully connected class of feed-forward (ANN) multilayer perceptron (MLP) has been employed to implement this task. The results successfully validate the proposed model, with a high matching rate in all scenarios. Having such a model is particularly relevant since it allows the straightforward implementation of advanced controllers easily and conveniently.

Table 6
Statistical platform pitch analysis.

Wind Speed (m/s)	Averages/Fluctuations (deg)	Control			Improvements	
		Uncontrolled with 4 closed Valves (deg)	Uncontrolled with 4 open Valves (deg)	Fuzzy Logic Control (deg)	FLC vs.Closed-valves (%)	FLC vs.Open-valves (%)
8	*avg*	1.4283	1.2187	1.5970	16.85	56
	δ	0.3844	0.7334	0.3196		
9	*avg*	1.4320	1.5524	1.3792	11.92	33.72
	δ	0.6045	0.8033	0.5324		
10	*avg*	1.8234	1.8970	1.6764	3.84	16.56
	Δ	0.7413	0.8542	0.7127		
11	*avg*	2.3493	2.1508	2.1476	9.90	13.3
	Δ	0.8559	0.8898	0.7711		
12	*avg*	2.9567	2.0799	2.6973	19.16	26.60
	Δ	0.9633	1.0609	0.7787		
13	*avg*	3.6348	2.4393	3.2949	11.18	46.56
	Δ	1.0595	1.7615	0.9413		
14	*avg*	4.3747	3.3113	4.0140	1.8445	50.98
	Δ	1.1331	2.2693	1.1122		
15	*avg*	5.1595	4.5230	4.8556	0	54.16
	Δ	1.1890	2.7148	1.2444		

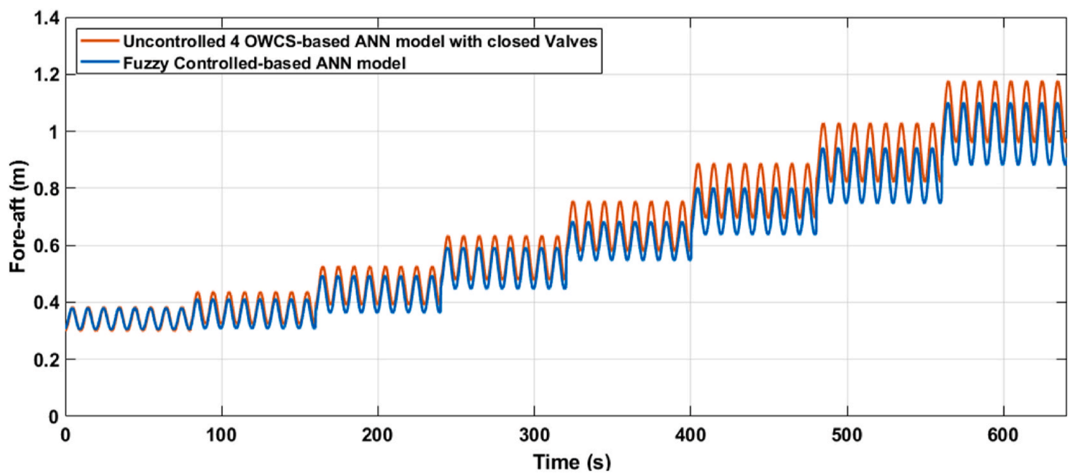

Fig. 26. Tower fore-aft displacement with FLC versus uncontrolled closed valves.

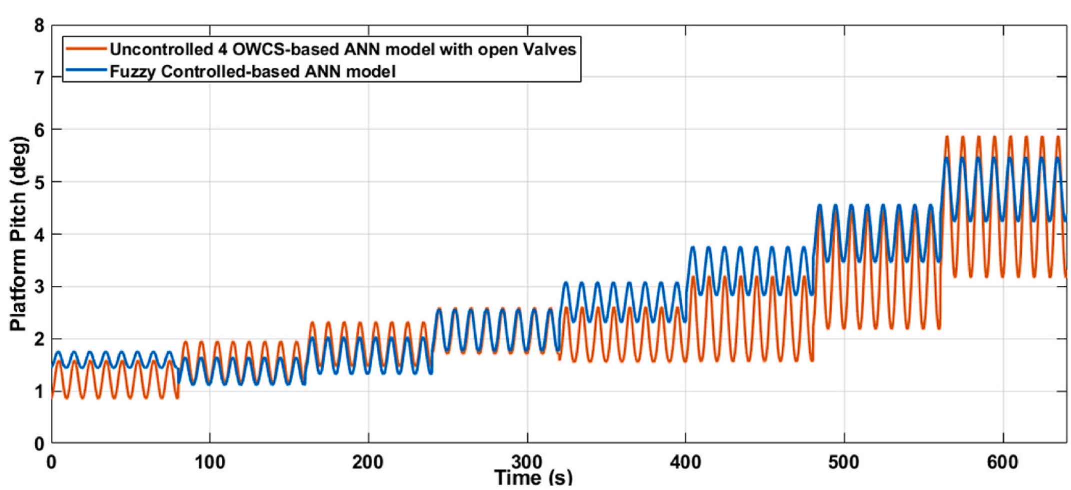

Fig. 27. Platform pitch angle with FLC versus uncontrolled open valves.

Secondly, once the model is established, an (FLC)-based controller is implemented to reduce the hybrid platform's undesired oscillations. This is achieved by adequately regulating the OWC airflow control valves to modulate the pressure drop within the OWC's air chambers.

The behavior of the controlled hybrid system is then compared with that of the uncontrolled case. Results show that the proposed control scheme affords a superior performance, successfully mitigating the platform pitch and top tower displacement and improving the platform

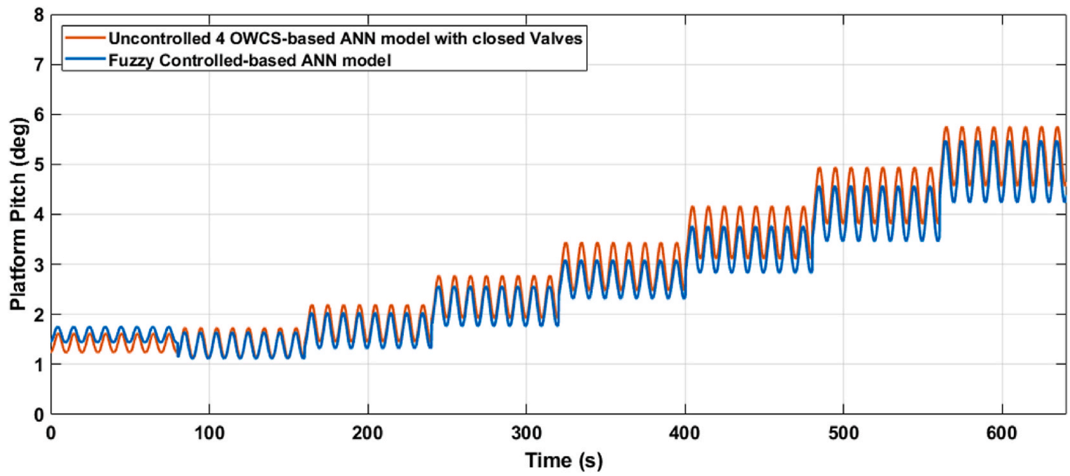

Fig. 28. Platform pitch angle with FLC versus uncontrolled closed valves.

stability.

Credit author statement

Irfan Ahmad: Conceptualization, Methodology, Software, Data Collection, and Manuscript-Writing. **Fares M'zoughi**: Conceptualization, Methodology, Software, Data Collection, Manuscript-Writing, and Proof-Reading. **Payam Aboutalebi**: Conceptualization, Methodology, Software, Data Collection, Manuscript-Writing, and Proof-Reading. **Izaskun Garrido***:* Conceptualization, Methodology, Software, Proof-Reading, and Supervision. **Aitor J. Garrido**: Conceptualization, Methodology, Software, Proof-Reading, and Supervision.

Declaration of competing interest

The authors declare that they have no known competing financial interests or personal relationships that could have appeared to influence the work reported in this paper.

Data availability

Data will be made available on request.

Acknowledgments

This work was supported in part by the Basque Government through project IT1555-22 and through the projects RTI2018-094902-B-C22 (MCIU/AEI/FEDER, UE), PID2021-123543OB-C21 and C22 funded by MCIN/AEI/10.13039/501100011033. The authors would also like to thank the UPV/EHU for the financial support through the Maria Zambrano grant MAZAM22/15 funded by the European Union-Next Generation EU and through grant PIF20/299.

Appendix A. Supplementary data

Supplementary data to this article can be found online at https://doi.org/10.1016/j.oceaneng.2022.113578.

References

Aboutalebi, P., M'zoughi, F., Garrido, I., Garrido, A.J., 2021. Performance analysis on the use of oscillating water column in barge-based floating offshore wind turbines. Mathematics 9 (5), 475.
Akinbami, O.M., Oke, S.R., Bodunrin, M.O., 2021. The state of renewable energy development in South Africa: an overview. Alex. Eng. J. 60 (6), 5077–5093.
Amundarain, M., Alberdi, M., Garrido, A.J., Garrido, I., 2011. Neural rotational speed control for wave energy converters. Int. J. Control 84 (2), 293–309.
Aubault, A., Alves, M., Sarmento, A.N., Roddier, D., Peiffer, A., 2011. Modeling of an oscillating water column on the floating foundation WindFloat. Int. Conf. Offshore Mech. Arctic Eng. 44373, 235–246.
Borg, M., Collu, M., Kolios, A., 2014. Offshore floating vertical axis wind turbines, dynamics modeling state of the art. Part II: mooring line and structural dynamics. Renew. Sustain. Energy Rev. 39, 1226–1234.
Bortolotti, P., Ivanov, H., Johnson, N., Barter, G.E., Veers, P., Namura, N., 2022. Challenges, opportunities, and a research roadmap for downwind wind turbines. Wind Energy 25 (2), 354–367.
Cadenas, E., Rivera, W., 2009. Short-term wind speed forecasting in La Venta, Oaxaca, México, using artificial neural networks. Renew. Energy 34 (1), 274–278.
Chang, G.W., Lu, H.J., Chang, Y.R., Lee, Y.D., 2017. An improved neural network-based approach for short-term wind speed and power forecast. Renew. Energy 105, 301–311.
Coudurier, C., Lepreux, O., Petit, N., 2015. Passive and semi-active control of an offshore floating wind turbine using a tuned liquid column damper. IFAC-PapersOnLine 48 (16), 241–247.
Dawoud, S.M., 2021. Developing different hybrid renewable sources of residential loads as a reliable method to realize energy sustainability. Alex. Eng. J. 60 (2), 2435–2445.
De O Falcão, A.F., Rodrigues, R.J.A., 2002. Stochastic modeling of OWC wave power plant performance. Appl. Ocean Res. 24 (2), 59–71.
Dinh, V.N., Basu, B., 2015. Passive control of floating offshore wind turbine nacelle and spar vibrations by multiple tuned mass dampers. Struct. Control Health Monit. 22 (1), 152–176.
Falcão, A.D.O., Justino, P.A.P., 1999. OWC wave energy devices with airflow control. Ocean Eng. 26 (12), 1275–1295.
Folley, M. (Ed.), 2016. Numerical Modeling of Wave Energy Converters: State-Of-The-Art Techniques for Single Devices and Arrays. Academic Press.
Goda, Y., 1999. A comparative review of the functional forms of the directional wave spectrum. Coast Eng. J. 41 (1), 1–20.
Guo, Yuzhu, et al., 2016. Ultra-orthogonal forward regression algorithms for the identification of nonlinear dynamic systems. Neurocomputing 173, 715–723.
Heath, T., Whittaker, T.J., Boake, C.B., 2001. The Design, Construction and Operation of the LIMPET Wave Energy Converter (Islay, Scotland)[Land Installed Marine Powered Energy Transformer].
IEA, Net renewable capacity additions by technology, 2017-2023, IEA, Paris https://www.iea.org/data-and-statistics/charts/net-renewable-capacity-additions-by-technology-2017-2023.
Jazayeri, K., Jazayeri, M., Uysal, S., 2016. Comparative analysis of Levenberg-Marquardt and Bayesian regularization backpropagation algorithms in photovoltaic power estimation using artificial neural network. In: Industrial Conference on Data Mining. Springer, Cham, pp. 80–95.
Jiménez, Arcos, Alfredo, Gómez Muñoz, Carlos Quiterio, García Márquez, Fausto Pedro, 2017. Machine learning for wind turbine blades maintenance management. Energies 11 (1), 13.
Jonkman, J.M., 2007. Dynamics Modeling and Loads Analysis of an Offshore Floating Wind Turbine. National Renewable Energy Lab. (NREL), Golden, CO, USA (No. NREL/TP-500-41958).
Jonkman, J.M., Buhl, M.L., 2005. FAST User's Guide, vol. 365. National Renewable Energy Laboratory, Golden, CO, USA, p. 366.
Jonkman, J., Butterfield, S., Musial, W., Scott, G., 2009. Definition of a 5-MW Reference Wind Turbine for Offshore System Development (No. NREL/TP-500-38060). National Renewable Energy Lab.(NREL), Golden, CO (United States).
Kaur, T., Kumar, S., Segal, R., 2016. Application of Artificial Neural Network for Short-Term Wind Speed Forecasting. In 2016 Biennial international conference on power and energy systems: towards sustainable energy (PESTSE), pp. 1–5. IEEE.
Khan, I., Zakari, A., Zhang, J., Dagar, V., Singh, S., 2022. A study of trilemma energy balance, clean energy transitions, and economic expansion in the midst of environmental sustainability: new insights from three trilemma leadership. Energy 248, 123619.

Kulkarni, S.S., Edwards, D.J., 2022. A bibliometric review on the implications of renewable offshore marine energy development on marine species. Aquaculture and Fisheries 7 (2), 211–222.
Lackner, M.A., Rotea, M.A., 2011a. Passive structural control of offshore wind turbines. Wind Energy 14 (3), 373–388.
Lackner, M.A., Rotea, M.A., 2011b. Structural control of floating wind turbines. Mechatronics 21 (4), 704–719.
Lin, Y.H., Kao, S.H., Yang, C.H., 2019. Investigation of hydrodynamic forces for floating offshore wind turbines on spar buoys and tension leg platforms with the mooring systems in waves. Appl. Sci. 9 (3), 608.
Lindh, R., Bernhardsson, A., Karlström, G., Malmqvist, P.Å., 1995. On the use of a Hessian model function in molecular geometry optimizations. Chem. Phys. Lett. 241 (4), 423–428.
Liu, Y., Wang, L., Gu, K., Li, M., 2022. Artificial Neural Network (ANN)-Bayesian Probability Framework (BPF) based method of dynamic force reconstruction under multi-source uncertainties. Knowl. Base Syst. 237, 107796.
López-Queija, J., Robles, E., Jugo, J., Alonso-Quesada, S., 2022. Review of control technologies for floating offshore wind turbines. Renew. Sustain. Energy Rev. 167, 112787.
Maria-Arenas, A., Garrido, A.J., Rusu, E., Garrido, I., 2019. Control strategies applied to wave energy converters: state of the art. Energies 12 (16), 3115.
McMorland, J., Collu, M., McMillan, D., Carroll, J., 2022. Operation and maintenance for floating wind turbines: a review. Renew. Sustain. Energy Rev. 163, 112499.
Men, Z., Yee, E., Lien, F.S., Wen, D., Chen, Y., 2016. Short-term wind speed and power forecasting using an ensemble of mixture density neural networks. Renew. Energy 87, 203–211.
Mishra, S.K., Appasani, B., Jha, A.V., Garrido, I., Garrido, A.J., 2020. Centralized Airflow Control to Reduce Output Power Variation in a Complex OWC Ocean Energy Network. Complexity, 2020.
M'zoughi, F., Aboutalebi, P., Garrido, I., Garrido, A.J., De La Sen, M., 2021. Complementary Airflow Control of Oscillating Water Columns for Floating Offshore Wind Turbine Stabilization. Mathematics 9 (12), 1364.
M'zoughi, F., Bouallegue, S., Garrido, A.J., Garrido, I., Ayadi, M., 2018. Fuzzy gain scheduled PI-based airflow control of an oscillating water column in wave power generation plants. IEEE J. Ocean. Eng. 44 (4), 1058–1076.
M'zoughi, F., Garrido, I., Garrido, A.J., De La Sen, M., 2020. Rotational speed control using ANN-based MPPT for OWC based on surface elevation measurements. Appl. Sci. 10 (24), 8975.
Noorollahi, Y., Jokar, M.A., Kalhor, A., 2016. Using artificial neural networks for temporal and spatial wind speed forecasting in Iran. Energy Convers. Manag. 115, 17–25.
Papi, F., Bianchini, A., 2022. Technical challenges in floating offshore wind turbine upscaling: a critical analysis based on the NREL 5 MW and IEA 15 MW Reference Turbines. Renew. Sustain. Energy Rev. 162, 112489.
Penalba, M., Kelly, T., Ringwood, J., 2017. Using NEMOH for Modeling Wave Energy Converters: A Comparative Study with WAMIT.
Ravinuthala, S., Das, S.K., Nithya, R., Das, S.P., 2022. Ocean, tidal and wave energy: science and challenges. Status and Future Challenges for Non-conventional Energy Sources 1, 1–21. Springer, Singapore.
Sacie, M., Santos, M., López, R., Pandit, R., 2022. Use of state-of-art machine learning technologies for forecasting offshore wind speed, wave and misalignment to improve wind turbine performance. J. Mar. Sci. Eng. 10 (7), 938.
Salcedo-Sanz, S., Pérez-Bellido, Á.M., Ortiz-García, E.G., Portilla-Figueras, A., Prieto, L., Paredes, D., 2009. Hybridizing the fifth-generation mesoscale model with artificial neural networks for short-term wind speed prediction. Renew. Energy 34 (6), 1451–1457.
Sarmiento, J., Iturrioz, A., Ayllón, V., Guanche, R., Losada, I.J., 2019. Experimental modeling of a multi-use floating platform for wave and wind energy harvesting. Ocean Eng. 173, 761–773.
Shah, S.A.A., Gao, B., Ahmed, N., Liu, C., 2021a. Advanced robust control techniques for the stabilization of translational oscillator with rotational actuator-based barge-type OFWT. Proc. IME M J. Eng. Marit. Environ. 235 (2), 327–343.
Shah, K.A., Li, Y., Nagamune, R., Zhou, Y., Rehman, W.U., 2021b. Platform Motion Minimization Using the Model.
Sheng, W., Li, H., Murphy, J., 2017. An improved method for energy and resource assessment of waves in finite water depths. Energies 10 (8), 1188.
Sierra-García, J.E., Santos, M., 2020. Performance analysis of a wind turbine pitch neuro controller with unsupervised learning. Complexity. https://www.hindawi.com/journals/complexity/2020/4681767/, 2020.
Sierra-García, J.E., Santos, M., 2021. Redes neuronales y aprendizaje por refuerzo en el control de turbinas eólicas. Revista Iberoamericana de Automática e Informática industrial 18 (4), 327–335.
Sitharthan, R., Devabalaji, K.R., Jees, Arun, 2017. A Levenberg–Marquardt trained feed-forward backpropagation based intelligent pitch angle controller for wind generation system. Renewable Energy Focus 22, 24–32.
Souissi, A., 2021. Optimum utilization of grid-connected renewable energy sources using the multi-year module in Tunisia. Alex. Eng. J. 60 (2), 2381–2393.
Stewart, G., Lackner, M., 2013. Offshore wind turbine load reduction employing optimal passive tuned mass damping systems. IEEE Trans. Control Syst. Technol. 21 (4), 1090–1104.
Tomin, N., Shakirov, V., Kozlov, A., Sidorov, D., Kurbatsky, V., Rehtanz, C., Lora, E.E., 2022. Design and optimal energy management of community microgrids with flexible renewable energy sources. Renew. Energy 183, 903–921.
Torre-Enciso, Y., Ortubia, I., De Aguileta, L.L., Marqués, J., 2009. Mutriku Wave Power Plant: from the Thinking Out to the Reality, vol. 710. In Proceedings of the 8th European wave and tidal energy conference, Uppsala, Sweden, pp. 319–329.
Torresi, M., Camporeale, S.M., Strippoli, P.D., Pascazio, G., 2008. Accurate numerical simulation of a high-solidity Wells turbine. Renew. Energy 33, 735–747.
Wilson, D.R., Martinez, T.R., 2003. The general inefficiency of batch training for gradient descent learning. Neural Network. 16 (10), 1429–1451.
Xu, X., Day, S., 2021. Experimental investigation on dynamic responses of a spar-type offshore floating wind turbine and its mooring system behavior. Ocean Eng. 236, 109488.
Zadeh, L.A., 1996. Fuzzy Sets. In Fuzzy Sets, Fuzzy Logic, and Fuzzy Systems: Selected Papers by Lotfi A Zadeh, pp. 394–432.
Zhang, Z., Høeg, C., 2021. Inerter-enhanced tuned mass damper for vibration damping of floating offshore wind turbines. Ocean Eng. 223, 108663.
Zhang, C., Gutierrez, S.V., Plestan, F., de León-Morales, J., 2019. Adaptive super-twisting control of floating wind turbines with collective blade pitch control. IFAC-PapersOnLine 52 (4), 117–122.
Zhang, D., Chen, Z., Liu, X., Sun, J., Yu, H., Zeng, W., et al., 2022. A coupled numerical framework for hybrid floating offshore wind turbine and oscillating water column wave energy converters. Energy Convers. Manag. 267, 115933.